Structure and Magnetic Properties of Bulk Synthesized $Mn_{2-x}Fe_xP_{1-y}Si_y$ Compounds from Magnetization, ^{57}Fe Mössbauer Spectroscopy, and Electronic Structure Calculations

Daniel Fruchart [1,*], **Sonia Haj-Khlifa** [1], **Patricia de Rango** [1], **Mohamed Balli** [2,3], **Ryszard Zach** [4], **Wieslaw Chajec** [4], **Piotr Fornal** [4], **Jan Stanek** [5], **Stanislaw Kaprzyk** [6,†] **and Janusz Tobola** [6]

[1] Institut Néel, CNRS et UGA, BP 166, 38042 Grenoble CÉDEX 9, France; soniahajkhlifa@gmail.com (S.H.-K.); patricia.derango@neel.cnrs.fr (P.d.R.)

[2] International University of Rabat, Parc Technopolis, Rocade Rabat-Salé 11100, Morocco; mohamed.balli@uir.ac.ma

[3] Institut Quantique, Département de Physique, Université de Sherbrooke, Sherbrooke, QC J1K 2R1, Canada

[4] Institute of Physics, Cracow University of Technology, Podchorazych 1, 30-084 Cracow, Poland; puzach@cyfronet.pl (R.Z.); wchajec@pk.edu.pl (W.C.); pufornal@cyf-kr.edu.pl (P.F.)

[5] M. Smoluchowski Institute of Physics, Jagiellonian Univiversity, Lojasiewicza 11, 30-348 Cracow, Poland; jan.stanek@uj.edu.pl

[6] AGH University of Science and Technology, Mickiewicza 30, 30-059 Cracow, Poland; kaprzyk@ftj.agh.edu.pl (S.K.); tobola@ftj.agh.edu.pl (J.T.)

* Correspondence: daniel.fruchart@neel.cnrs.fr

† Deceased end October 2018 when completing this work dedicated to Stanek, a high level and gentleman scientist.

check for
updates

Abstract: The series of $Mn_{2-x}Fe_xP_{1-y}Si_y$ types of compounds form one of the most promising families of magnetocaloric materials in term of performances and availability of the elemental components. Potential for large scale application needs to optimize the synthesis process, and an easy and rather fast process here described is based on the use of two main type of precursors, providing the Fe-P and Mn-Si proportions. The series of $Mn_{2-x}Fe_xP_{1-y}Si_y$ compounds were synthesized and carefully investigated for their crystal structure versus temperature and compared interestingly with earlier results. A strong magnetoelastic effect accompanying the 1st order magnetic transition—as well as the parent phosphide–arsenides—was related to the relative stability of both the Fe magnetic polarization and the Fe–Fe exchange couplings. In order to better understand this effect, we propose a local distortion index of the non-metal tetrahedron hosting Fe atoms. Besides, from Mn-rich (Si-rich) to Fe-rich (P-rich) compositions, it is shown that the magnetocaloric phenomenon can be established on demand below and above room temperature. Excellent performance compounds were realized in terms of magnetic entropy ΔS_m and adiabatic temperature ΔT_{ad} variations. Since from literature it was seen that the magnetic performances are very sensitive to the synthesis process, correspondingly here a new effective process is proposed. Mössbauer spectroscopy analysis was performed on Mn-rich, equi-atomic Mn-Fe, and Fe-rich compounds, allowing determination of the distribution of hyperfine fields setting on Fe in the tetrahedral and pyramidal sites, respectively. Electronic structure calculations confirmed the scheme of metal and non-metal preferential ordering, respectively. Moreover, the local magnetic moments were derived, in fair agreement with both the experimental magnetization and the Fe contributions, as determined by Mössbauer spectroscopy.

Keywords: ternaries $Mn_{2-x}Fe_xP_{1-y}Si_y$; bulk synthesis; tetrahedra distortion; magnetic characteristics magnetocaloric properties; ^{57}Fe Mössbauer spectroscopy; electronic structure analysis

1. Introduction

The series of pnictides related to the Fe_2P type, which we have studied for a long time, exhibit very unusual magnetic properties, as detailed in a series of reports [1–3]. In fact, these ternary compounds TT'X (T, T' = transition metals, X = P, As, Si, Ge etc.) crystalize in one of three types of structures: orthorhombic (SG Pnma: O4), hexagonal (SG P-62m: H3), and tetragonal (SG $P4_2$/nmm: T2). The polytype structures, from the most to the least dense compacting modes of a unique Rhombus (R) block (with 4, 3, and 2 blocks successively), are formed from two X-tetrahedrons and two-X-pyramids coordinating T and T' [1,4]. The compaction level of the structure directly impacts the magnetic characteristic of the polytypic series when T and T' share magnetic trends. In fact, the tetragonal compounds, being mostly arsenides (X = As), exhibit antiferromagnetic (AF) characteristics [4,5], while the orthorhombic compounds, being mostly phosphides, exhibit typically non-collinear and long range magnetic ordering [6,7]. For the intermediately dense compounds of hexagonal Fe_2P type structure, ferromagnetic (Ferro) and long-range magnetic structures are observed. These typical behaviors were effectively found with the $MnFeP_{1-x}As_x$ [4] system, where in successive orthorhombic, hexagonal, and tetragonal structures, Mn occupies the CN5-coordinated site (pyramid: PYR) and Fe occupies the CN4-coordinated one (tetrahedron: TET). The non-collinear MnFeP AF-type of magnetic structure was solved in a simple orthorhombic AF-2c cell, but from more precise neutron diffraction data, a long-range magnetic ordering was established with M_{Mn} = 3.07 μ_B and M_{Fe} ~ 0.13 μ_B [7,8]. Besides, a O4 to H3 process was found occurring versus temperature [9].

The tetragonal, less dense MnFeAs was established early as having a collinear AF structure [5], then confirmed in [10] with M_{Mn} = 3.36 μ_B and M_{Fe} ~ 0.0 μ_B. Under high pressure, a denser hexagonal (P-62m) MnFeAs compound was stabilized and parallel experimental and electronic structure investigations revealed that both Mn and Fe share a magnetic moment with M_{Mn} = 3.14 μ_B and M_{Fe} = 1.54 μ_B, respectively [10]. Similarly, according to the increasing relative density of polytypes from T2 to H3 to O4, it is worth recalling that under pressure, the ferromagnetic H3 Fe_2P was transformed to a ferromagnetic O4 form [11]. If the Curie temperature was slightly diminished (by ~5 K), the hyperfine fields (~Fe moments) were markedly reduced (0.75 for PYR and 0.5 for TET sites). Obviously, similar transformations were recently found occurring in the $Fe_2P_{1-y}Si_y$ system under high pressure [12].

For 0.15 < x < 0.66, the $MnFeP_{1-x}As_x$ system crystallizes within the hexagonal P-62m symmetry with Mn and Fe in 3g and 3f positions, respectively. X = P, As, occupy 1 and 2c positions [4]. According to size and electronegativity differences [1,13], the site selectivity [14–16] is respected and for the equi-atomic Mn/Fe composition, only a very little amount of metal disorder was noticed, but some P to As redistributions were found. A first order AF-F transition accompanied with a marked magnetoelastic effect was evidenced in the hexagonal $MnFeP_{1-x}As_x$ system. This transition line (P-rich side), where almost no volume change occurs ($\Delta a/a \sim -1/2\ \Delta c/c$), was found in the prolongation of the ferromagnetic to paramagnetic (Para) transition line (P-poor side). The long range incommensurate magnetic structure of the AF-type was solved only thanks to information gained both by neutron diffraction and ^{57}Fe Mössbauer spectroscopy [14–16]. It consists in both Mn-helix and Fe-sine arrangements with M_{Mn} = 2.40 μ_B and M_{Fe} = 0.45 μ_B, respectively. Such a complex magnetic structure was confirmed more recently [17]. The magnetic moment of Fe appears highly sensitive to the overall magnetic structure, the same as for the critical Fe_2P [2,16–19]. In contrast to the large Mn moment of 2.6–3.02 μ_B, that of Fe is found to be more than twice as large in the ferromagnetic state (1.20 μ_B) than in the AF state [13]. Moreover, the Fe moment is expected to depolarize in the paramagnetic state, in fair agreement with DFT-based calculations for Fe_2P and $(Fe_{2-x}Ru_x)_2P$ [20]. Accordingly, the reverse susceptibility markedly deviates from a typical Curie-Weiss law supported by short range ordering [4,14,16,21], suggesting a Moriya spin fluctuation regime [22] that was more recently confirmed by μ^+SR investigations [23]. It is worth recalling that all hexagonal Fe_2P type magnetic materials forming a 2D stacking mode of Mn/Fe layers exhibit a strong deviation from a linear $1/\chi$ behavior versus temperature, being in contrast with the parent orthorhombic Pnma compounds, which exhibit an overall random Mn-vs.-Fe distribution within a 3D network [4,24].

More interestingly, very outstanding properties were revealed in terms of magnetocaloric (MC) characteristics [25], then promoting the series of $Mn_{2-x}Fe_xP_{1-y}As_y$ compounds among the best-known MC materials susceptible of application in magnetic refrigeration at room temperature. Following this discovery, an increasing number of papers have been published [17,26,27]. However, because of the negative aspect of arsenic in such compounds that are considered for domestic application, efforts to substitute this poisoning element (e.g., by silicon or Ge) have been carried out while successfully preserving high magnetocaloric effect (MCE) levels [28–30]. Again, a considerable interest was raised for the parent series of $Mn_{2-x}Fe_xP_{1-y}Si(Ge)_y$ compounds, with both experimental and theoretical knowledge gained on structural and magnetic properties of the novel series [31–40].

The aim of the present contribution is not to provide an additional review report on the $Mn_{2-x}Fe_xP_{1-y}Si(Ge)_y$ compounds, for which considerable literature can be found for the last ten years, and exciting fundamental results and potentially high application properties were pointed out and for a part referenced in [41–49].

Based on lengthy practice and knowledge of the "generic" phosphide–arsenide series (not only comprising Mn and Fe as d-magnetic metals [3]), we aimed focus on three main aspects to account for better knowledge of the new $Mn_{2-x}Fe_xP_{1-y}Si_y$ series. These are:

-       A local structure distortion index which can affect the tetrahedral site in which the sensitive Fe-metal (weak-ferro versus strong-ferro character), possibly linking the magnetic correlations with magnetoelastic couplings;
-       Optimized route to process intermetallic materials, comprising amounts of phosphorous, easily and safely, to deliver bulk samples with high magnetocaloric performances;
-       Better understanding the magnetic properties from correlated Mössbauer spectroscopy and electronic structure calculations.

For that, apart from the equi-atomic $MnFeP_{0.5}Si_{0.5}$, we have focused both on Fe-poor and Fe-rich compounds, with some variation on the P versus content, since the ratios Mn/Fe and P/Si are effective for drastically monitoring the Curie temperature via exchange couplings, steric effects, etc.

2. Materials and Methods: On Synthesis Routes

The used method to synthesize the ternary phosphides and arsenides was the conventional route of solid-state reaction, where the powder of the considered elements are intimately mixed then placed in an evacuated silica ampoule and annealed at optimized temperatures of reaction that are usually higher than 1100 °C [4,6,7,24]. However, although this technique was successfully employed in the past, its utilization in certain cases is delicate, particularly because of the high vapor pressure of phosphorus at low temperatures, as well as the transformation of its red to white allotropic form occurring close to 450 °C [24,33]. On the other hand, it is worthy to recall that the efforts to perfectly substitute and combine silicon to the TT'X series were made unsuccessful using solid-state reaction routes, even after several months of high temperature treatments [6]. Effectively, at temperature high enough to expect the compounds to homogenize by annealing treatments, traces of binary or ternary based silicide impurities remained visible, since the formation enthalpy of Si-octahedral coordinated T-element appears more favorable than that of the tetrahedral site of the here considered hexagonal (and isotype) TT'X compounds [1]. In order to overpass the associated difficulty with the phosphorus vapor pressure, a group of Amsterdam University has successfully proceeded to low temperature solid-state synthesis by mechanical alloying using the ball milling (BM) method [25–27]. Next, the BM method has allowed realization of the low temperature substitution of arsenic by silicon (and Ge) to synthesize the isotype $Mn_{2-x}Fe_xP_{1-y}Si(Ge)_y$ compounds [25,26,29]. It was confirmed that almost pure ternary compounds can be achieved only if Si occupies at maximum the 2c site, with P being restricted to the 1b site [12,30,34]. However, the BM procedure is not an effective route to prepare economically large amounts of MC materials. Additionally, production of extra fine particles before the annealing

step needs to process very carefully the BM powders. For more details about recent developments regarding the practical aspects of Fe$_2$P-type materials, we refer to the references [50,51].

Besides taking advantage of the atomization technique [28], several kgs of Mn$_{2-x}$Fe$_x$P$_{1-y}$Si$_y$ samples were synthesized as nano-crystalline powders using a Fe-P precursor and complementary amounts of Mn, Fe, and Si [35,36]. Unfortunately, some P-rich deposits were found in the condensation chamber, even after various annealing procedures, while it was highly challenging to obtain these materials in a single hexagonal phase. The resulting magnetic characteristics (not described here) were found to be far from those previously reported in the literature (e.g., synthesized by BM).

Next, various Fe-P precursors used as additives in steel metallurgy were tested for their relative stability at high temperature, since their formula is closer to a eutectic composition and contains binary phosphides Fe$_2$P and FeP. Tiny amounts of Fe$_3$P can be detected by microanalysis [36]. Tests of P-pressure vapor were conducted using Ta and Nb targets during the HF heating to melt Fe$_2$P or MnFe(P-Si), unveiling the formation of both TaP and NbP. Conversely, the same targets did not react in similar conditions when using pure Fe$_2$P [36]. Therefore, the synthesis of a perfect and well crystallized Fe$_2$P sample can be carried out from the Fe-P precursor and the corresponding addition of cleaned ~20–40 μm Fe-particles, by way of either solid state reaction or induction heating techniques. Next, stoichiometric and well crystallized Mn$_3$Si and Mn$_5$Si$_3$ were easily prepared by induction melting. Finally, combinations of these high-quality primaries Fe$_2$P, Mn$_5$Si$_5$, and Mn$_3$Si in calculated amounts, with a few complements of pure Fe, Mn, or Si if requested, has led to easy synthesis of the Mn$_{2-x}$Fe$_x$P$_{1-y}$Si$_y$ compounds, restricting y close to $\leq$2/3 for the optimum repartition of P and Si at the 1b and 2c sites of the P-62m type structure [36]. A two-step process means that first binary precursors are prepared by induction melting, thus stabilizing their own compositions, and second a ternary material is melted with limited risks of decomposition.

Then, an annealing procedure for 2–3 h at T > 1150 °C allows delivery of pure H3-type materials, provided that cooling was fast enough. Several parent compounds, such as those discussed in the present paper (Mn$_{1.40}$Fe$_{0.60}$P$_{0.30}$Si$_{0.70}$, Mn$_{1.30}$Fe$_{0.70}$P$_{0.35}$Si$_{0.65}$, MnFeP$_{0.50}$Si$_{0.50}$, Mn$_{0.70}$Fe$_{1.30}$P$_{0.65}$Si$_{0.35}$, and Mn$_{0.60}$ Fe$_{1.40}$P$_{0.60}$Si$_{0.40}$), were synthesized, using this easy induction melting procedure of Fe-P and Mn-Si based precursors [36]. Recently, batches of ~12 kg of (Mn-Cr)FeP$_{1-y}$Si$_y$ were successfully prepared according to the two steps method, starting with a commercial Fe$_{80}$P$_{20}$ and different Mn$_5$Si$_3$ and Mn$_3$Si-type precursors prepared aside. A small amount of Cr was used to tailor the ordering temperature [37].

3. Results

3.1. Structure Analysis

3.1.1. Structure Characterization at Room Temperature

For all compounds discussed here, XRD patterns were recorded using a reflexion diffractometer Siemens d5000R (Siemens, Berlin and Munich, Germany) and a transmission diffractometer. The reflexion diffractometer (R) working at λ_K (Co) = 1.791 Å is equipped with a backscattering graphite (0002) monochromator and the transmission diffractometer (T) working at λ_K (Cu) = 1.5412 Å is equipped with a Ge (111) backscattering monochromator. Typical diffraction patterns of MnFeP$_{0.50}$Si$_{0.50}$ (a) and Mn$_{0.6}$ Fe$_{1.4}$P$_{0.6}$Si$_{0.4}$ (b) are shown Figure 1.

From a profile refinement method, the metal atom positions and co-ordinations were found to be in good agreement with literature [25–30]. The structure parameters of both samples are reported Table 1. Appendix A: Figure A1 shows the structure and Table A1 set inter-atomic distance examples.

If the compounds appear to be almost pure and well crystallized, the X-ray diffraction technique does not allow refining with either the metal or the non-metal atom distribution or disorder between their respective two possible crystal sites, 3f and 3g on one side and 1b and 2c on the other side. In Table 1 the relative occupancies are attributed according to the experimental rules reported in [1,13],

being in agreement with the more recent literature. However, few metal and non-metal disorders can be expected, as was mentioned in [28,29,31,34,36].
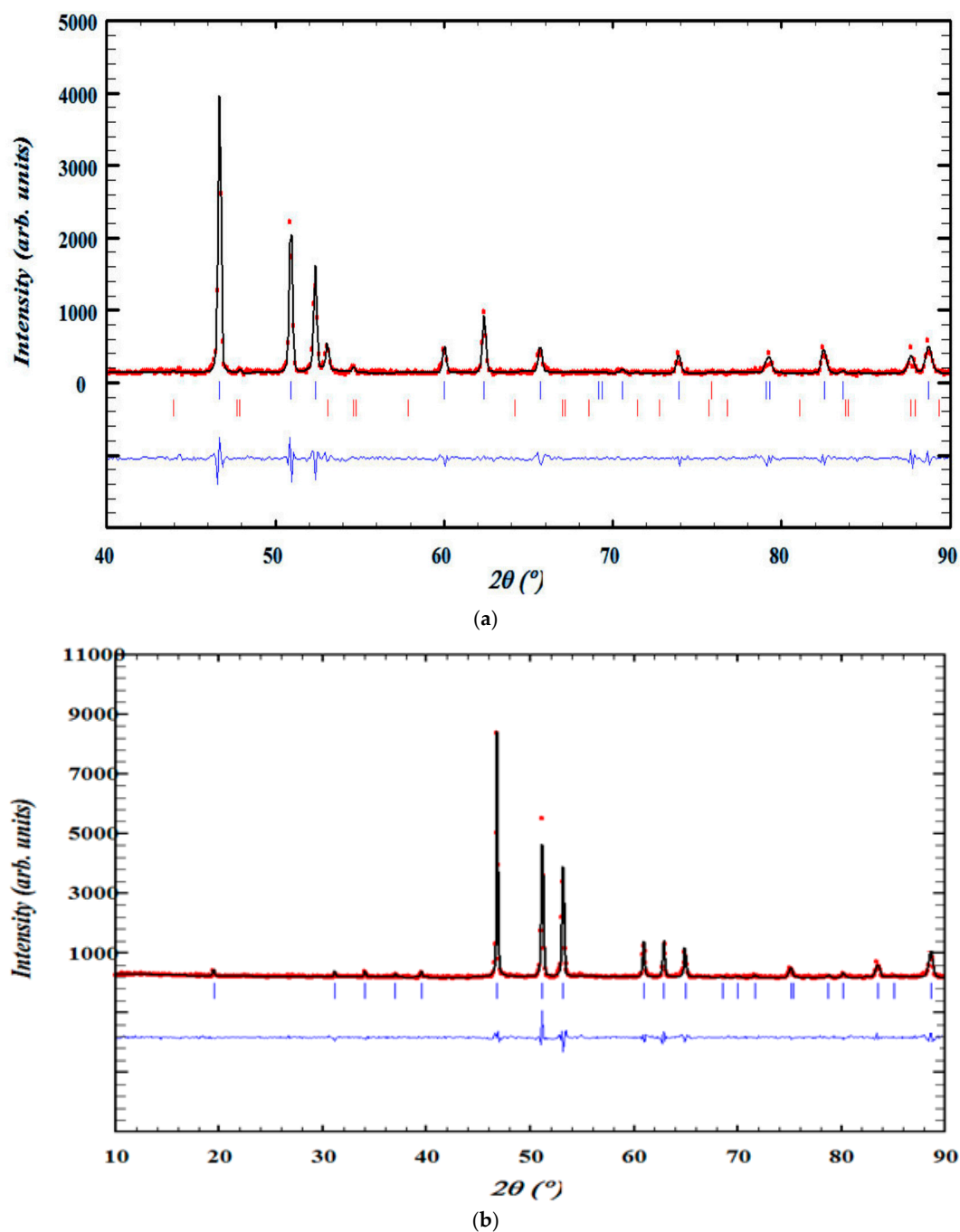

(a)

(b)

Figure 1. Examples of XRD patterns for (**a**) $MnFeP_{0.5}Si_{0.5}$, where Bragg lines are indicated by blue ticks. A small % of silicide impurity $MnFe_6Si$ is indicated by red ticks. (**b**) $Mn_{0.6}Fe_{1.4}P_{0.6}Si_{0.4}$ > 99% pure.

Table 1. Structural parameters of $MnFeP_{0.5}Si_{0.5}$ (**I**) and $Mn_{0.6}Fe_{1.4}P_{0.6}Si_{0.4}$ (**II**).

Sites	Sample I	x	y	z	Sample II	x	y	z
3g	100% Mn	0.5967(1)	0.0	0.5	56% Mn + 44% Fe	0.598(8)	0.0	0.5
3f	100% Fe	0.2491(2)	0.0	0.0	100% Fe	0.268(6)	0.0	0.0
2c	P,Si	0.33333	0.66666	0.0	100% P	0.33333	0.66666	0.0
1b	P,Si	0.0	0.0	0.5	33.3% P + 66.6% Si	0.0	0.0	0.5

For these compounds, as for the other ones synthesized by induction melting using Fe-P and Mn-Si precursors, a few percent's impurities—if present (e.g., $Mn_2Fe_3Si_3$ or $MnFe_2Si$ type)—were identified using parallel JCPDS files (Joint Committee on Powder Diffraction Standards), thermomagnetic analysis (Curie temperature), and as SEM ZEISS-Ultra (Carl Zeiss, Oberkochen, Germany) + type JEOL JSM-840A (JEOL, Ltd. Akishima, Japan) equipped with Oxford EDX microanalysis (Oxford Instruments plc, Abingdon, UK) The cell parameters at room temperature and the purity level of the phases are shown in Table 2.

Table 2. Extra phases identified in $Mn_{2-x}Fe_xP_{1-y}Si_y$ synthesized by melting Fe-P and Mn-Si precursors.

Compounds	% Fe_2P-Type (P-62m)	% Mn_5Si_3-Type (P6$_3$/mcm)	Cell Parameters (Å)
$Mn_{1.40}Fe_{0.60}P_{0.30}Si_{0.70}$	91	9	a = 6.139, c = 3.425
$Mn_{1.30}Fe_{0.70}P_{0.35}Si_{0.65}$	96	4	a = 6.053, c = 3.355
$MnFeP_{0.50}Si_{0.50}$	96	~4% $MnFe_2Si$	a = 6.196, c = 3.309
$Mn_{0.70}Fe_{1.30}P_{0.65}Si_{0.35}$	99	<1	a = 6.101, c = 3.347
$Mn_{0.60}Fe_{1.40}P_{0.60}Si_{0.40}$	99	<1	a = 6.123, b = 3.334

3.1.2. Structure Characterization versus Temperature

To investigate the structures behavior versus temperature, a X'PERT PRO MPD PANalytical (PW-3710) θ-2θ diffractometer was used at λ_K (Cu) = 1,5412 Å with a backscattering graphite (0002) monochromator (Malvern, Almelo, The Netherlands).

Two Anton Paar systems have enabled us to control the temperature of the samples within ±0.5 K. This ancillary equipment, filled with 5N purity Ar gas, are a TTK for temperatures ranging from 90 to 300 K and an HTK for temperatures ranging from 300 to above 500 K. Figure 2 presents a succession of XRD patterns recorded as a function of temperature for $MnFeP_{0.5}Si_{0.5}$. The crystal parameters a and c are found to markedly change their values in the temperature range 374–384 K.
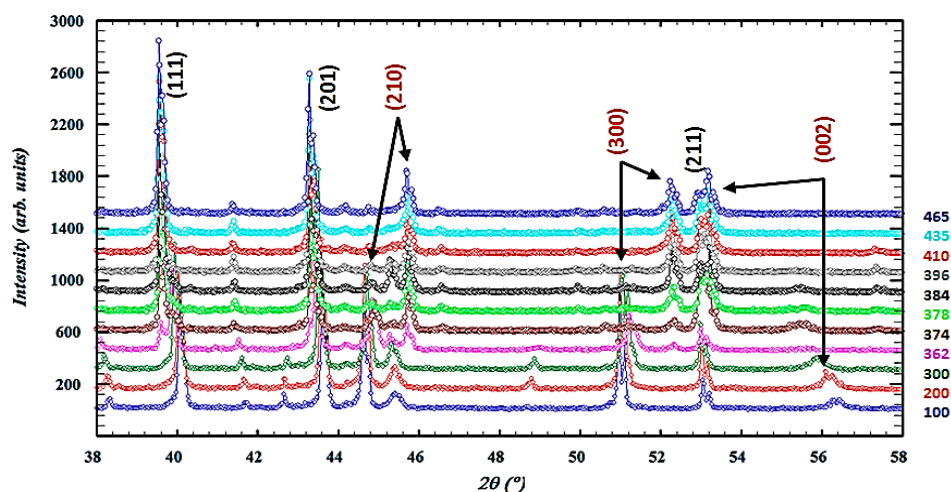

Figure 2. XRD patterns recorded on $MnFeP_{0.5}Si_{0.5}$ for temperatures ranging between 100 and 465 K. For clarity, only half of the patterns are plotted. The first order magnetic phase transition occurs in the 274–284 K range. Extra small lines belong to the $MnFe_2Si$ impurities, as mentioned in Figure 1a and reported in Table 2.

Using the collection of XRD patterns recorded versus temperature, as shown in Figure 2, the cell parameters a (T), c (T), and the volume V (T) were determined and represented in Figure 3 (e.g., for $MnFeP_{0.5}Si_{0.5}$ and Figure 4 for $Mn_{0.7}Fe_{1.3}P_{0.65}Si_{0.35}$). The magnetoelastic effect illustrated here is quite similar to what was earlier reported for the $MnFeP_{1-y}As_y$ system [4,14] and then confirmed later in many works dedicated to $Mn_{2-x}Fe_xP_{1-y}Si_y$ compounds [15–17,25].

Additionally, similar magnetoelastic behaviors were observed in the isotype series of $Mn_{2-x}Fe_xP_{1-y}Si_y$ compounds [30]. These are typical characteristics of the deep crystal structure modifications accompanying a first order magnetic phase transition, usually leading to a strong magnetocaloric effect [25]. In all cases, the hexagonal cell compresses abruptly by ~1.5% in the basal plane, it expands by ~3% along the c-axis, and correspondingly there is almost no change of the cell volume [25,36].
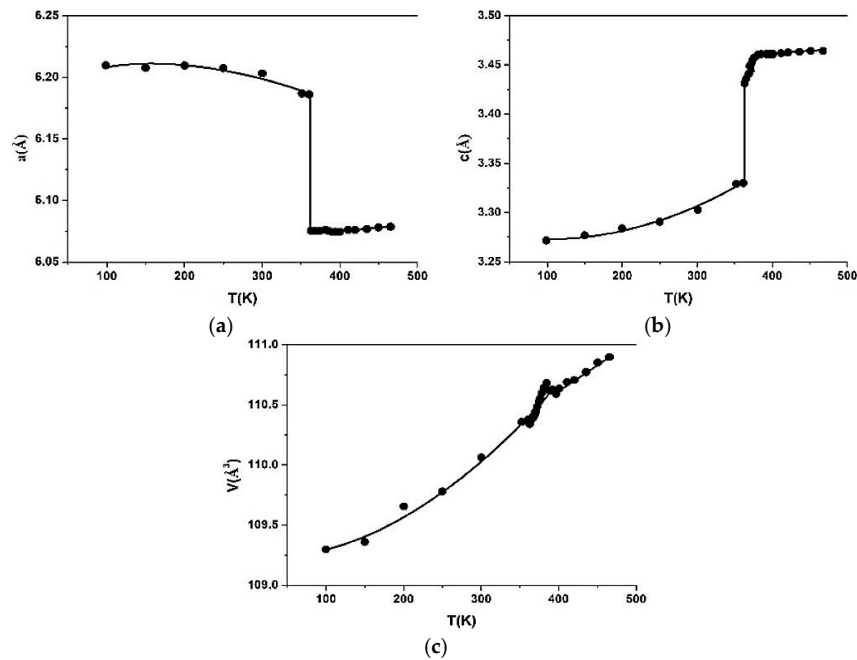

Figure 3. Thermal variation of the cell parameters for $MnFeP_{0.5}Si_{0.5}$: (**a**) a-cell parameter; (**b**) c-cell parameter; (**c**) cell volume.
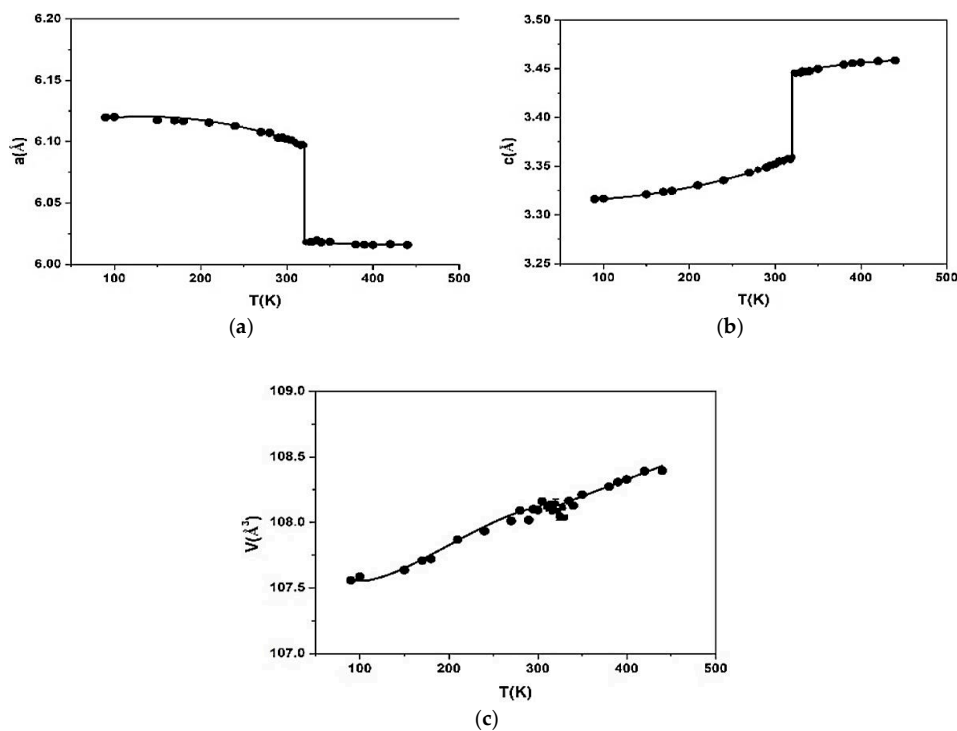

Figure 4. Thermal variation of the cell parameters for $Mn_{0.7}Fe_{1.3}P_{0.65}Si_{0.35}$: (**a**) a-cell parameter; (**b**) c-cell parameter; (**c**) cell volume.

3.1.3. Local Structure Distortion Index and Magnetic Polarization

When studying in details 4 isotypic compounds MnRuP, MnRuAs, MnRhP and MnRhAs, also comparing their crystal and magnetic parameters to the other hexagonal TT'X phosphides and arsenides, several general characteristics have been noticed [7]. Since, and specially for the hexagonal H3 polytype the cell volume is given as:

$$V_{Hex} = 3V_R = 3(2V_{PYR} + 2V_{TET}), \text{ where } V_{PYR} = a^2 \cdot c \cdot \sqrt{3}/18 \text{ and } V_{TET} = a^2 \cdot c \cdot \sqrt{3}/36 \tag{1}$$

It was shown [7] that for a given transition metal atom T' (e.g., Ru) occupying the TET site, the relative variation of V_{TET} can reach 14% while for Mn preferentially occuping the PYR site (according to the general rules depicted in [1,3]) the relative volume variation of V_{PYR} (when changing the metal T') is less, at most 9.5% [7]. In fact, the tetrahedral site is distorted: the in-plane edge joining 2 non-metal neighbors X(2c) being written as d_{2c-2c} (or p for planar edge) and the axial edge length d_{1b-1b} (axial edge, equal to the c cell-parameter) allows define a TET-distortion coefficient:

$$\delta = d_{(2c-2c)}/d_{(1b-1b)} - 1 \tag{2}$$

The δ (%) measured values in several phosphides and arsenides in ref [7] are as different as +4.07 for MnRuAs (F), +2.43 for MnRuP (AF) and, −2.29 for ZrRuAs (non-magnetic). According to criteria (2), additionally to Figures 3 and 4 quantifying the magnetoelastic phenomenon in the hexagonal $Mn_{2-x}Fe_xP_{1-y}X_y$ (X = As, Si, Ge) known to exhibit large MCEs, we have represented the thermal behavior of δ (otherwise called dp/da − 1) for the two of here studied compounds in Figure 5. If all the calculated interatomic distances exhibit some anomalous but tedious variation at Tc, Figure 5 shows that the δ index involving the distortion of the TET site provides very pertinent information that supports the strong magnetoelastic effect accompanying the magnetic phase transition. As a confirmation, we have verified that in the $MnFeP_{1-y}As_y$ series, a fairly similar anomaly in $\delta(T)$ to that measured (e.g., for $MnFeP_{0.5}Si_{0.5}$ as shown in Figure 5) takes place in the $MnFeP_{0.65}As_{0.35}$ compound. Appendix A—Table A2 displays some inter-atomic distances at 300 and 465 K for $MnFeP_{0.5}Si_{0.5}$ where appears that distances related to the tetrahedron are of the most modified.
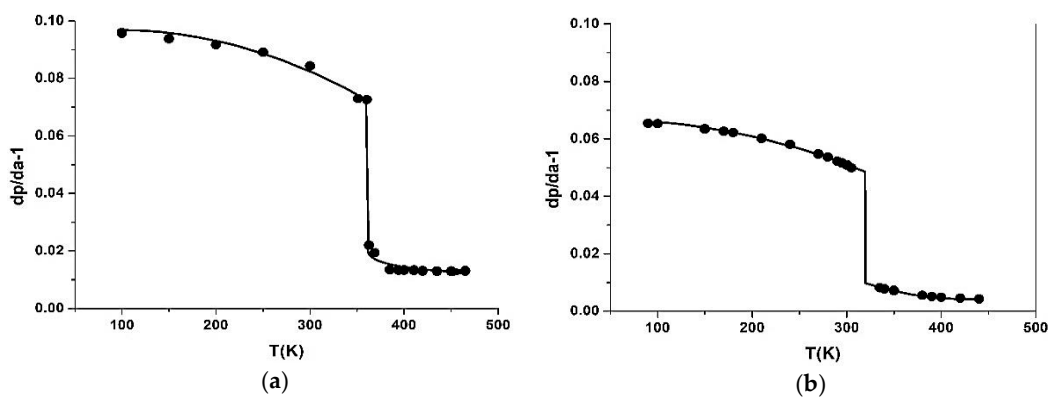

Figure 5. The $\delta(T) = dp/da - 1$ index traces for (**a**) $MnFeP_{0.5}Si_{0.5}$ and (**b**) $Mn_{0.7}Fe_{1.3}P_{0.65}Si_{0.35}$.

Abrupt changes of the TET site dimensions, here mostly occupied by Fe, should be ascribed to the magnetic polarization instability of the Fe (TET) that consequently affects the strength of the MCE. According to crystal electric field (CEF) considerations [38], the tetrahedral symmetry of the CEF leads to the degeneracy of the d shell to form a doublet $(d3z^2\text{-}r^2) - (dx^2\text{-}y^2)$ of lower energy and a triplet (dxy) − (dyz) − (dzx) containing the non-appaired electrons [7]. The distortion of the tetrahedral sites raises partly the degeneracy of the later orbital states, which would induce variations of the local (Fe mainly) magnetic moment. The existence of a magnetoelastic effect directly correlated to the degree of distortion of the TET site allows understanding the fundamental mechanisms behind the magnetic

polarization of Fe (uniquely or mainly) occupying this site. In the TT′X series, there is no specific metal to non-metal distance, since both the PYR and TET volumes vary with the nature of the T′ atom. Consequently, the deformation of the TET site is mainly related to the nature of the T and T′ atoms [7].

Recently, the hypothesis of a CEF splitting was re-considered via DOS-partial resolution of S and P-levels, after pointing out the inequivalent distances of Fe-Si and Fe-P around the TET site [12]. In fact, this latest derivation was said to be inconclusive, since the 3d electrons are engaged in different types of bonding—moreover, with the metal neighbors too. However, it is worth recalling that the distortion of the TET site is not specific to phosphide-silicides, but also to phosphide-arsenides, and pure phosphides and arsenides.

In the (ferromagnetic) MnT′X phosphides and arsenides, Mn preferentially occupying the PYR sites shares a markedly high magnetic moment of ~3.0 μ_B. In contrast, since Fe prefers to occupy the TET site, it shares a much smaller magnetic moment of less than 2 μ_B. Upon the magnetoelastic phenomenon occurring at a first order critical temperature, the magnetic moment of Mn appears moderately affected. Conversely, the magnetic moment of Fe can severely drop down (e.g., F to AF transition in $MnFeP_{1-x}As_x$) [15]; it can even completely collapse, the same as for the Ferro-Para transitions of $MnFeP_{1-x}As_x$ [14,15], $MnFeP_{1-x}Si_x$ [34], and $Fe_{2-x}Ru_xP$ systems [10,20]. In terms of magnetic correlations, as investigated using neutron diffraction or ^{57}Fe Mössbauer spectroscopy [14–16], it results in long range AF magnetic orderings in the first case, and it evidences in the second case a magnetic scattering up to temperatures far above the so-called Curie temperature [14,40]. For the presently studied compounds, we consider the situation is made somewhat different (1) because of the more metallic character of Si reference to P(As) and (2) because of the preferential occupancy of the 2c sites by Si, when P occupies the 1b site. Consequently, the hexagonal crystal structure appears, forming a 2D stacking of (001) planes, with the Mn-P planes alternating with Si(P)-Fe ones. The main crystallographic and magnetic features corresponding to the cases of $Mn_{2-x}Fe_xP_{1-y}Si_y$ are considered in a following chapter dedicated to their electronic structure calculations.

3.2. Magnetization Properties and MCE Characteristics of Bulk Synthesized $Mn_{2-x}Fe_xP_{1-y}Si_y$ Compounds

Magnetization characterizations have been performed using two extraction-type magnetometers by integrating a magnetic flux variation in a series/opposition system of bi-coils. The low temperature equipment allows collection of the magnetization data over a temperature range from 1.5 to 320 K in 0 to 10 T fields generated by a superconducting magnet. The high temperature equipment provides a magnetic field span from 0 to 7 T, enabling us to record magnetization over the temperature range between 200 and 850 K. The resolution of both magnetometers is better than 10^{-7} Am^2. The records that allow determination of the transition temperature were operated under a weak magnetic field (typically 0.05 T), while the saturation magnetization was systematically recorded at 5 K. In order to determine the magnetic entropy variation, a set of magnetic isotherms were recorded by steps of 2 to 5 K (depending on the temperature range) under fields up to 10 T. The data were used to deliver the MCE in terms of the entropy change via a numerical integration of the well-known Maxwell relation given by [52]:

$$\Delta S_m(T,\ H_2 - H_1) = -\int_{H_1}^{H_2} \left(\frac{\partial M}{\partial T}\right)_H dH \tag{3}$$

The adiabatic temperature change can be evaluated according to the following equation:

$$\Delta T_{ad}\ (T, H2 - H1) = -\int_{H1}^{H2} \frac{T}{C_{P,H}} \mu_0 \left(\frac{\partial M}{\partial T}\right)_H dH \tag{4}$$

A Quantum Design PPMS equipped with a 0–9 T superconducting coil was used to determine $C_{p,H}$ at constant pressure. The magnetic contribution to the specific heat (assuming a negligible contribution of the electronic term) was determined by using a non-magnetic reference, the polytype phosphide Co_2P

(assuming a similar phonon contribution). Furthermore, direct measurements of ΔT_{ad} were performed using homemade equipment developed at Néel Institute with the support of the company CoolTech Applications (Holtzheim, France). However, in order to deliver real quantitative comparisons, this type of measurement needs disposal of strictly well shaped and similar sized samples [53].

3.2.1. Tc Determination and Isothermal Magnetization Measurements

Examples of magnetic ordering temperature, as determined by application of a 0.05 T field and plotting the derivative of the magnetization traces, are displayed in Figure 6. It appears that for both Mn-rich and Si-rich compounds, the ordering temperature falls down to room temperature, while for Fe-rich and P-rich formula, the compounds order above room temperature. In fact, the highest ordering temperatures were found occurring with the equi-atomic Mn/Fe and Si/P compositions, being comprised between 365 and 390 K, depending on the stoichiometry and the experienced annealing procedure by the samples.
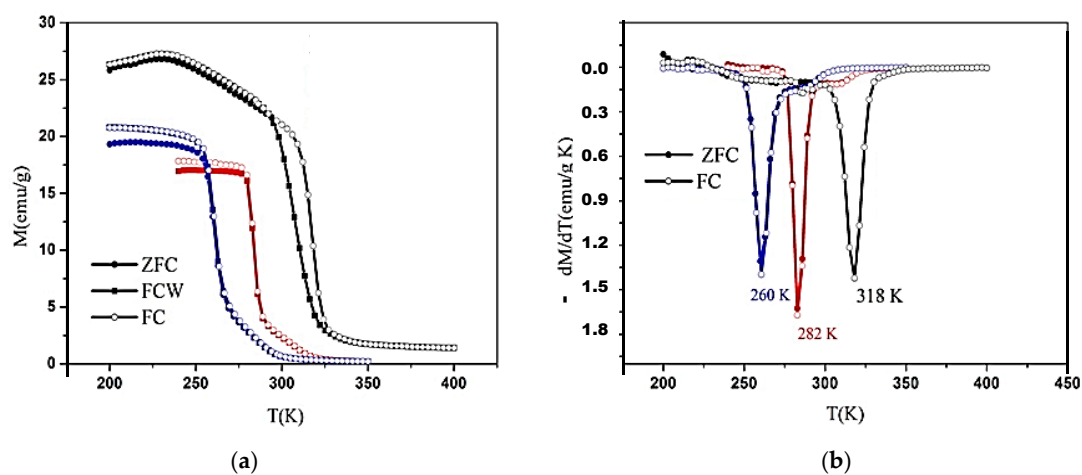

Figure 6. (**a**) Temperature dependence of magnetization for 3 selected compounds. Zero-field-cooled and field-cooled ($\mu_0 H = 0.05T$) indicate the possible hysteresis effect at the magnetic transition region; (**b**) derivatives of thermomagnetic curves that enables us to accurately determine the transition temperature—black: $Mn_{0.7}Fe_{1.3}P_{0.65}Si_{0.35}$; red: $Mn_{1.3}Fe_{0.7}P_{0.35}Si_{0.65}$; blue: $Mn_{1.4}Fe_{0.6}P_{0.30}Si_{0.70}$.

3.2.2. MCE Characterizations

Systematic magnetic isotherms were recorded in the temperature range around the ordering temperature on all the studied compounds. Figure 7 illustrates these records for both Mn- and Si-rich and Fe- and P-rich formula (i.e., $Mn_{1.4}Fe_{0.6}P_{0.3}Si_{0.7}$, $Mn_{1.3}Fe_{0.7}P_{0.35}Si_{0.65}$, and $Mn_{0.7}Fe_{1.3}P_{0.65}Si_{0.35}$). Interestingly the latter compound exhibits a more pronounced metamagnetic character. The highest saturation level corresponds to the equi-atomic metal and non-metal formula, displaying also the highest Curie temperature, as reported in Table 3. According to Equation (3), the change of magnetic entropy was numerically derived for all the compounds and represented in Figure 8, which is compared to the equi-atomic compound of $MnFeP_{0.50}Si_{0.50}$ formula. However, for clarity, the entropy change is only reported in Figure 8b for 0 to 1 T and 0 to 5 T field variations.

The mostly ferromagnetic exchange forces issued from the Fe sites and a marked balance between F and AF couplings, leading to a global metamagnetic behavior, was observed and deeply discussed in several papers as one of the main magnetic characteristics of the $Mn_{2-x}Fe_xP_{1-y}X_y$ series (with X = As, Si, Ge) [14–16,23,29,30,32,42–46].

To determine the adiabatic temperature variation ΔT_{ad} using Equation (4), specific heat measurements were undertaken under a zero-magnetic field as well as under magnetic fields by using Quantum Design PPMS facilities. In order to estimate the magnetic field contribution only, the non-magnetic and parent reference pnictide Co_2P was measured first. Figure 9a shows the three

C_P measurements under a zero-magnetic field for $Mn_{1.3}Fe_{0.7}P_{0.35}Si_{0.65}$, $Mn_{0.7}Fe_{1.3}P_{0.65}Si_{0.35}$, and Co_2P (as a reference). The magnetic contributions to the total specific heat are plotted in Figure 9b for the two Mn-Fe phosphide-silicides. Finally, the adiabatic temperature variations were determined for the same samples and shown in Figure 10a. In Figure 10b is displayed the ΔT_{ad} experienced by the $MnFeP_{0.5}Si_{0.5}$ under several magnetic field variations, for comparison.
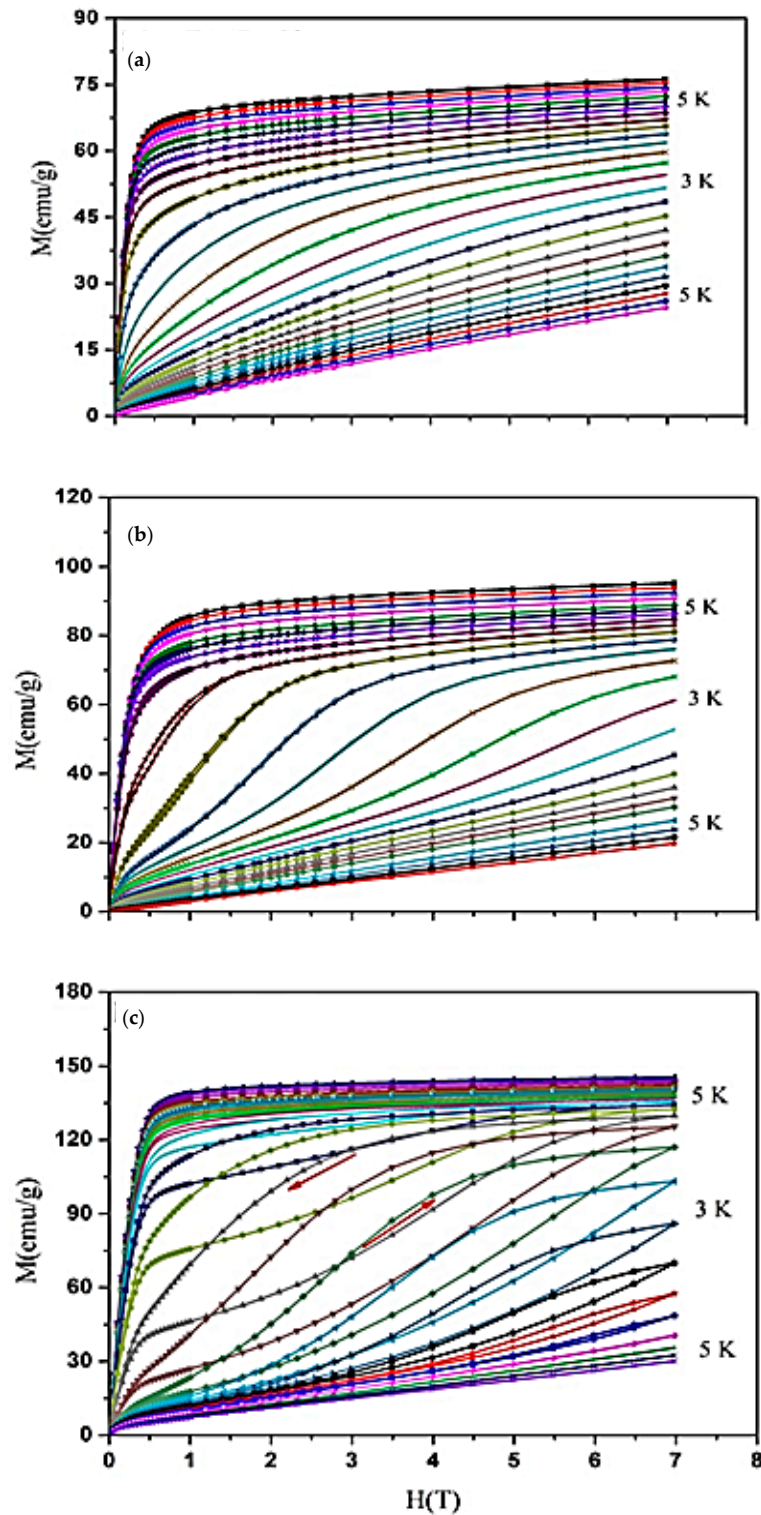

Figure 7. Magnetic isotherms: for (**a**) $Mn_{1.4}Fe_{0.6}P_{0.3}Si_{0.7}$, (**b**) $Mn_{1.3}Fe_{0.7}P_{0.35}Si_{0.65}$, (**c**) $Mn_{0.7}Fe_{1.3}P_{0.65}Si_{0.35}$.
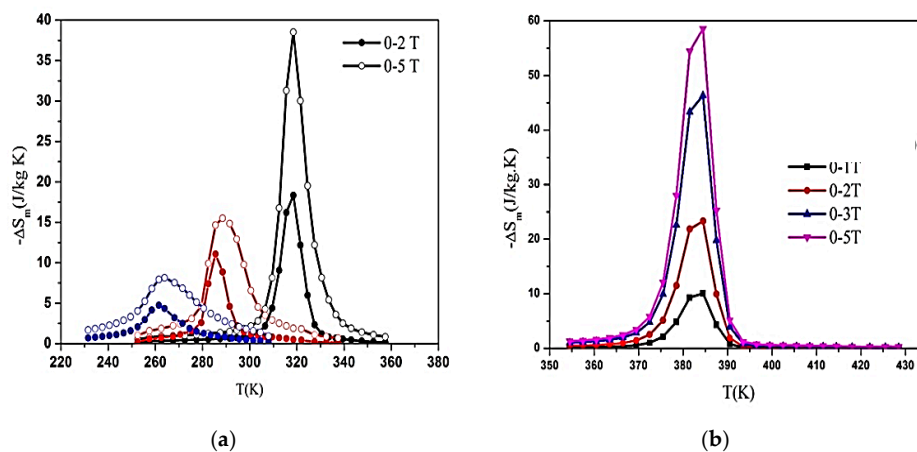
Figure 8. Magnetic entropy variation ΔS_m for (**a**) $Mn_{1.4}Fe_{0.6}P_{0.3}Si_{0.7}$ (blue) $Mn_{1.3}Fe_{0.7}P_{0.35}Si_{0.65}$ (red) and $Mn_{0.7}Fe_{1.3}P_{0.65}Si_{0.35}$ (black) under 0–2 T (black dots) and 0–5 T (open circles) magnetic field shifts, respectively; (**b**) $MnFeP_{0.5}Si_{0.5}$ for several magnetic field shifts.
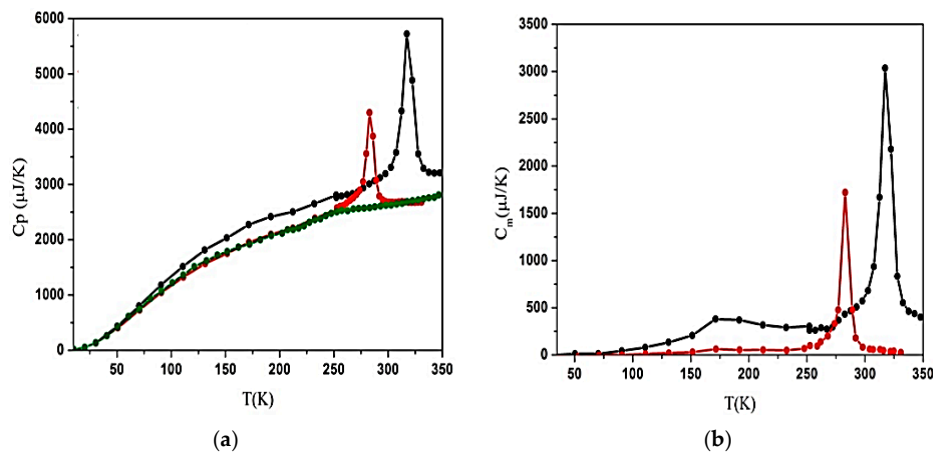
Figure 9. Specific heat measurements (here under zero-field) as performed on members of the series. $Mn_{2-x}Fe_xP_{1-y}Si_y$ compared to a non-magnetic parent phosphide Co_2P (**a**) for Co_2P (green), $Mn_{1.30}Fe_{0.70}P_{0.30}Si_{0.70}$ (red), $Mn_{0.70}Fe_{1.30}P_{0.65}Si_{0.35}$ (black) (**b**) after subtracting the Co_2P contribution.
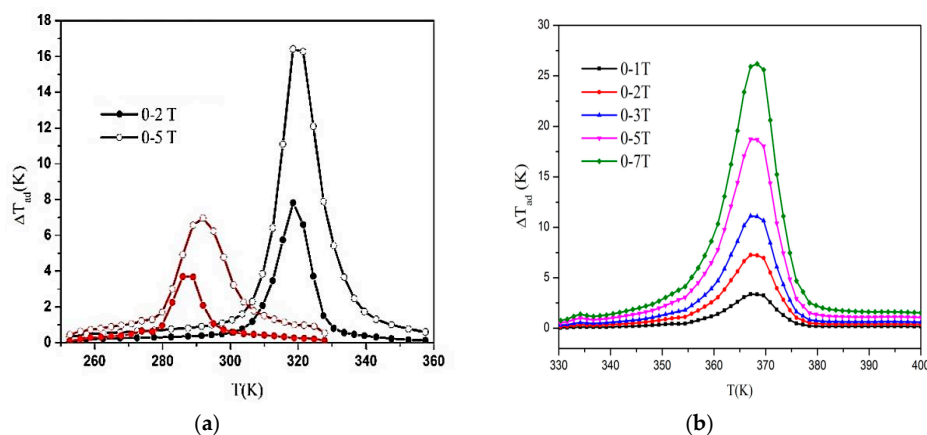
Figure 10. Adiabatic temperature determination for (**a**) $Mn_{1.3}Fe_{0.7}P_{0.35}Si_{0.65}$ (red) and $Mn_{0.7}Fe_{1.3}P_{0.65}Si_{0.35}$ (black) under 0–2 T (black dots) and 0–5 T (open circles) magnetic field variations respectively and (**b**) $MnFeP_{0.5}Si_{0.5}$ for several magnetic field shifts.

The magnetic and magnetocaloric characteristics are displayed in Table 3. According to the latter, it can be seen that from the magnetization analysis at 5 K, $Mn_{1.30}Fe_{0.70}P_{0.35}Si_{0.65}$ and

$Mn_{0.70}Fe_{1.30}P_{0.65}Si_{0.35}$ exhibit reduced Ms values when compared to other members of the series. In fact, a superimposed "susceptibility" (slope) for about 5% in magnetization was found for fields varying from 0 to 10 T. One can anticipate that some AF couplings could have taken place for these two samples, breaking an easy approach to the saturation state. All the values reported in Table 3 agree with those determined earlier by Ou and Dung for $Mn_{2-x}Fe_xP_{1-y}Si_y$ compounds having similar or close compositions (e.g., by the group of Delft) [41,43,49].

For the equi-atomic formula $MnFeP_{0.50}Si_{0.50}$, the reported values in Table 3 correspond to two "interesting" samples (* and **) that were prepared with little changes in the precursor combination. After the annealing procedure, it appears that this formula could rapidly unveil different magnetic characteristics, as shown in Figure 11 for ΔS_m variations. This means that the nominal composition, the effective resulting composition, and the annealing conditions can play a very important and critical role in the real distribution of metal and non-metal elements at their respective crystal sites. These aspects could impact significantly the expected final magnetic characteristics, as reported and discussed in [45,48]. Appendix A—Figure A2 shows for atomized and highly disordered $MnFeP_{0.50}Si_{0.50}$ samples, no magnetoelastic effect is observed at T_C in agreement with that is shown Figure 11.

Table 3. Main magnetic and magnetocaloric characteristics measured on six members of the series $Mn_{2-x}Fe_xP_{1-y}Si_y$ versus decreasing values of the Mn/Fe ratio, * and ** samples are explicated Figure 11.

Compound	Fe/Mn	Si/P	Transition Order	T_C (K)	M_S (μ_B)	ΔT hys (K)	$-\Delta S_m^{max}$ (J/kg K) 2 T–5 T	ΔT_{ad} (K) 2 T–5 T
$Mn_{1.40}Fe_{0.60}P_{0.30}Si_{0.70}$	2.333	2.333	F→P 1–2nd (?)	260	4.17	0	4.63–8.3	-
$Mn_{1.30}Fe_{0.70}P_{0.35}Si_{0.65}$	1.858	1.858	MET 1st	282	>2.87	0	11–15.5	3.6–6.8
$MnFeP_{0.50}Si_{0.50}$ *	1.0	1.0	MET 1st	365	3.95	18	15–30	7.6–20
$MnFeP_{0.50}Si_{0.50}$ **	1.0	1.0	MET 1st	382	3.77	18	24–58	8–16.1
$Mn_{0.70}Fe_{1.30}P_{0.65}Si_{0.35}$	0.538	0.538	MET 1st	318	>3.25	10	18.4–38	7.8–16.4
$Mn_{0.60}Fe_{1.40}P_{0.60}Si_{0.4}$	0.428	0.666	F→P 1–2nd (?)	394	4.05	6	4.1–8.5	1.1–2.5
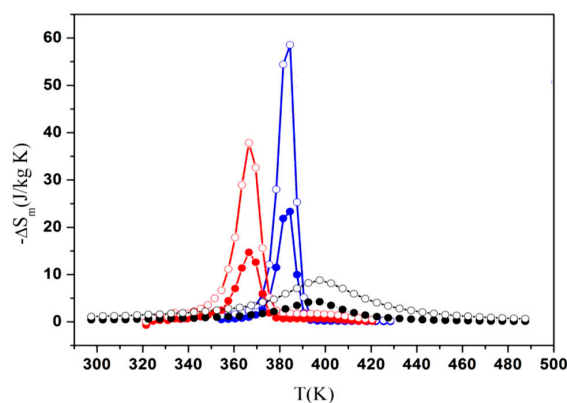
Figure 11. The ΔS_m variations of three $MnFeP_{0.50}Si_{0.50}$ samples: black dots for atomized powder [35], red dots for Fe-P + Mn-Si precursors only (*), and blue dots for atomized powders + complementary precursors (**) [36], dots are for [0–2 T] and circles are for [0–5 T] magnetic shifts, respectively.

3.3. ^{57}Fe Mössbauer Spectroscopy Analysis

Several types of hexagonal and orthorhombic TT′X compounds have been successfully quantified in terms of site occupancy and magnetic polarization by using the ^{57}Fe Mössbauer spectroscopy [4,6,10,13,15,16,54–57].

Here, three compounds were selected to probe the local magnetic properties of the $Mn_{2-x}Fe_xP_{1-y}Si_y$ series from Fe-poor to Fe-rich sides (i.e., $Mn_{1.4}Fe_{0.6}P_{0.3}Si_{0.7}$, $MnFeP_{0.5}Si_{0.5}$, and $Mn_{0.7}Fe_{1.3}P_{0.65}Si_{0.35}$) by using ^{57}Fe Mössbauer spectroscopy. The spectra were recorded in transmission geometry in a bath cryostat at temperatures T = 310, 250, 200, 150, and 84 K. The temperature stabilization was 0.1 K. The obtained spectra were fitted using MOSSMOD or WinNorm programs, assuming two or three local Fe sites, characterized by isomer shift and quadrupole splitting values within each site. A Gaussian distribution of the magnetic hyperfine field was assumed. The spectra recorded between 84 and 310 K exhibited distributions of the hyperfine magnetic fields acting on the Fe located at tetrahedral 3f or pyramidal 3g sites of the hexagonal structure. The impact of the local non-metal (P and Si) and metal (Mn and Fe) neighborhood of Fe in terms of magnetic properties was investigated. At first, the influence of the 50% substitution of Si to P at the 2c position of the $Mn_{2-x}Fe_xP_{1-y}Si_y$ structure on the Fe local magnetic characteristics was examined. For the equi-atomic composition, in principle Fe exclusively occupies the 3f position, while Mn occupies the 3g position [6,13–16,36,57]. Then, modifications of the magnetic intra- and inter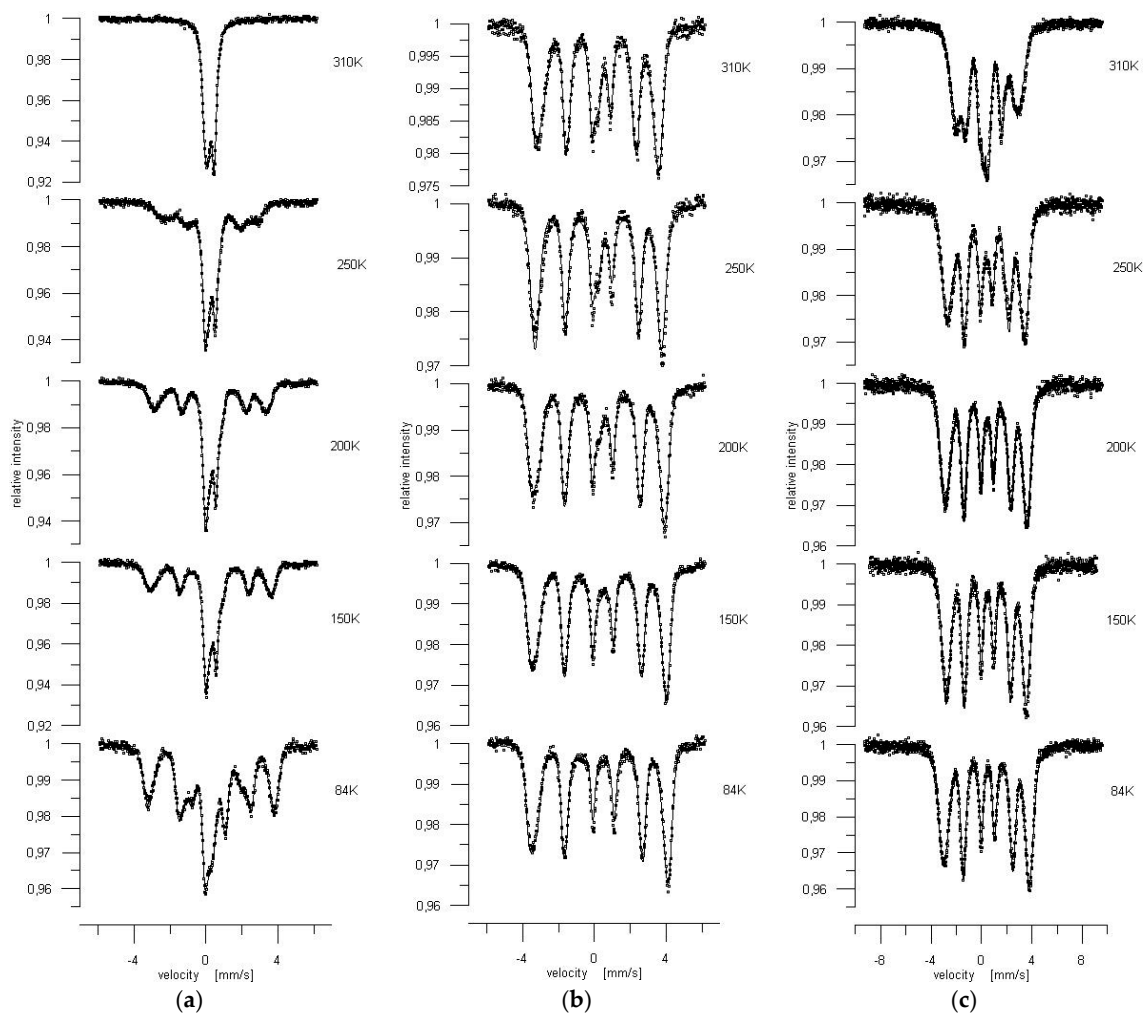-atomic correlation of Fe by nearest Fe metal neighbors were studied in $Mn_{1.4}Fe_{0.6}P_{0.3}Si_{0.7}$, where 40% of Mn substitutes to Fe at the 3f position and reciprocally in $Mn_{0.7}Fe_{1.3}P_{0.65}Si_{0.35}$, where 30% of Fe substitutes to Mn at the 3g position.

3.3.1. Results

The recorded spectra and the corresponding distributions of the hyperfine fields for the studied compounds are shown in Figure 12, from Fe-poor to Fe-rich formulas. The hyperfine parameters and the relative contributions of the fractions are collected in Table 4. For $MnFeP_{0.5}Si_{0.5}$ (equi-atomic composition) the distribution of the magnetic field may be formally reproduced by the sum of two Gaussians with different isomer shifts. However, above 150 K, a small contribution of paramagnetic fraction of ~7% can be seen. The spectra of the Fe-poor $Mn_{1.4}Fe_{0.6}P_{0.3}Si_{0.7}$ are more complicated. At 84 K the entire distribution of the magnetic field may be reproduced by three Gaussians centered on significantly different values of average magnetic fields. Between 150 and 250 K, the spectra consist of one magnetic and two paramagnetic patterns. At 310 K, all the Fe moments are in a paramagnetic state.

Table 4. Results of Mössbauer studies of the Fe-poor $Mn_{1.4}Fe_{0.6}P_{0.3}Si_{0.7}$ (columns 2 to 6), the equi-atomic compound $MnFeP_{0.5}Si_{0.5}$ (columns 7 to 11), and the Fe-rich $Mn_{0.7}Fe_{1.3}P_{0.65}Si_{0.35}$ (columns 12 to 16). Symbols are: T—temperature [K], <B>—average value of hyperfine field in the Gaussian distribution [T], σ—half-width distribution [T], IS—isomer shift vs. metallic iron [mm/s], QS quadrupole splitting [mm/s], and P—contribution [%].

T	<B>	σ	IS	QS	P	<B>	σ	IS	QS	P	<B>	σ	IS	QS	P
	0	0	0.23	0.41	49	21.6	2.3	0.28	−0.22	49	16.2	3.3	0.29	0.25	64
310	0	0	0.20	0.59	11	0	0	0.19	0	11	13.9	3.6	0.36	0.23	18
	0	0	0.17	0	40	19.5	2.8	0.32	−0.13	40	0	0	0.28	0.30	18
	15.6	4.0	0.29	−0.18	50	22.6	2.4	0.31	−0.22	50	19.3	3.0	0.37	0.06	72
250	0	0	0.24	0.58	10	0	0	0.23	0	10	16.1	3.6	0.44	0.1	21
	0	0	0.17	0	40	20.8	2.6	0.37	−0.12	40	0	0	0.30	0.29	7
	19.1	3.3	0.33	−0.19	40	23.3	2.1	0.34	−0.23	40	20.3	2.9	0.40	0.15	77
200	0	0	0.29	0.59	7	0	0	0.23	0	7	18.7	2.7	0.47	0.10	23
	0	0	0.19	0	53	21.5	2.5	0.39	−0.14	53					
	20.6	3.0	0.36	−0.19	43	23.8	2.1	0.37	−0.23	43	19.9	2.8	0.41	0.14	77
150	0	0	0.29	0.59	10	0	0	0.29	0	10	18.6	2.5	0.48	0.07	23
	0	0	0.19	0	47	21.9	2.5	0.42	−0.14	47					
	21.6	2.7	0.40	−0.21											
84	9.5	3.2	0.31	0.25	45	24.2	2.0	0.39	−0.24	45	21.3	2.9	0.45	−0.15	77
	1.9	2.5	0.21	0.07	55	22.4	2.6	0.44	−0.14	55	19.5	2.6	0.52	0.07	23

Figure 12. Transmission spectra of: (**a**) the Fe-poor compound $MnFeP_{0.5}Si_{0.5}$; (**b**) the equi-atomic compound $Mn_{1.4}Fe_{0.6}P_{0.3}Si_{0.7}$; and (**c**) the Fe-rich compound $Mn_{0.7}Fe_{1.3}P_{0.65}Si_{0.35}$, measured at different temperatures.

The spectra of the Fe-rich $Mn_{0.7}Fe_{1.3}P_{0.65}Si_{0.35}$ below room-temperature were fitted by two magnetic sub-spectra with a Gaussian distribution of the magnetic fields with significantly different isomer shifts. At 250 K, one additional paramagnetic component was observed.

3.3.2. Data Analysis

The aim of the present Mössbauer spectra analysis is elucidation of the impact of the local surrounding Fe atoms on their magnetic properties. The analysis is divided into three steps. First, we discuss the role of the different non-metal Si and P configurations ($MnFeP_{0.5}Si_{0.5}$), and next the similar role of d-metal (Fe, Mn,) configurations for the Mn-rich ($Mn_{1.4}Fe_{0.6}P_{0.3}Si_{0.7,}$) and the Fe-rich ($Mn_{0.7}Fe_{1.3}P_{0.65}Si_{0.35}$) samples. For $MnFeP_{0.5}Si_{0.5}$, iron in the tetrahedral position may be coordinated by 2P-2Si, 3P-1Si, and 4P-0Si atoms. In the case of $Mn_{1.4}Fe_{0.6}P_{0.3}Si_{0.7}$, the ratio P/Si is very close to $\frac{1}{2}$, and consequently there is almost one type tetrahedron formed by 2P-2Si. For the third studied compound, namely $Mn_{0.7}Fe_{1.3}P_{0.65}Si_{0.35}$, there are three types of tetrahedral sites with co-ordinations 2P-2Si, 3P-1Si, and 4P-0Si. In fact, it is seen that these different non-metal configurations weakly modify the hyperfine magnetic field but influence the s-electron density at the Fe nuclei, causing asymmetry of the Zeeman patterns, formally reproduced in the fitting procedure of the $MnFeP_{0.5}Si_{0.5}$ spectra by the assumption of two magnetic sub-spectra. A similar result was reported for $MnFeP_{1-x}As_x$ [15,16].

The role of the Fe neighboring d-metal atoms is decisive for its magnetic state and consequently for the resulting exchange forces. For $Mn_{1.4}Fe_{0.6}P_{0.3}Si_{0.7}$, Fe located at the 3f site has two nearest metal atoms (3f site) at 2689 Å [36]. Three different local configurations must be distinguished for Fe_{3f}: two Fe atoms with the probability $0.6 \times 0.6 = 0.36$, two Mn atoms with the probability $0.4 \times 0.4 = 0.16$, and one Fe and Mn atom with the probability $2 \times 0.6 \times 0.4 = 0.48$. The next nearest and next-next nearest metal atoms are Mn only, located at 3g site. Such local configurations are seen as the three different magnetic fields observed at 84 K. The fraction with a hyperfine field of about 21 T should be assigned to the Fe-Fe-Fe configuration, as with $MnFeP_{0.5}Si_{0.5}$. It is interesting to recall that in the case of $Mn_{1.4}Fe_{0.6}P_{0.5}As_{0.5}$, three similar magnetic sub-spectra were found [6,58].

The Mn atoms at 3f sites weaken the ferromagnetic-mode coupling of the Fe magnetic moments and lowers the Curie point of the system, which is in agreement with the magnetic susceptibility measurements [18,57]. For the iron rich compound $Mn_{0.7}Fe_{1.3}P_{0.65}Si_{0.35}$, the spectra were decomposed into two sextets, assigned to two Fe sites. The component with significantly higher isomer shift and relative intensity of ~23% (see Table 4) should be assigned to the Fe at the 3g position. The distribution of the magnetic field in both sites, due to the different local metal atom arrangement, is found weaker than that in the case of $Mn_{1.4}Fe_{0.6}P_{0.3}Si_{0.7}$. The Mössbauer spectroscopy investigations allow pointing out various magnetic states of Fe in the series. This may be explained by the different local metal atom configurations when varying the Mn/Fe ratio. For the equi-atomic compound $MnFeP_{0.5}Si_{0.5}$, Mn, and Fe are almost assigned to 3g and 3f positions, respectively, and Si exclusively occupies the 2c position. An almost regular distribution of magnetic interactions leads to support for the highest ordering temperature and the largest hyperfine field on the Fe 3f-site. Besides which, the variation of the P/Si ratio in the range 0.33–1 has a relatively weak impact on the Fe magnetic polarization and exchange couplings comparison made with the direct impact of relative occupation of the 3f and 3g by Fe and Mn respectively, namely when Fe occupies the octahedral 3f site.

According to a rather general relationshi experimentally found in such metal-type compounds formed between 3d and non-metal elements (such as Si, P, As, etc.) [59], one can estimate the local magnetic moment of Fe using the correspondence $1 \mu_B \sim 14$ T. The values deduced for Fe_{3f} are found in good agreement with what is anticipated from electronic structure calculations, as reported in Table 5. Table 6 allows compare the magnetic moments values of Mn and Fe with those found for parent hexagonal MnFeX (X = As; $P_{0.5}As_{0.5}$, $P_{0.7}As_{0.3}$). Interestingly, it appears that for the P-Si systems (Table 5), the calculated magnetic polarization on Mn_{3g} (Fe_{3f}) decreases (increases) by 0.2–0.3 μ_B. This opposite changes should be related to the change of electronic configuration 3p2 (Si) to 3p3 (P, As) and relative electronegativity and not to a change of size of the non-metal atoms since approximately the radii are as 1, 1.1 and 1.2 Å for P, Si and As respectively. This seems supporting well, the impact of a CEF scheme, leading to a critical increase of the experimental saturation magnetization reported from Table 5 to Table 6.

Table 5. Total (per formula) and site-decomposed magnetic moments (per atom) in selected compounds of $Mn_{2-x}Fe_xP_{1-y}Si_y$, as calculated from Korringa Kohn Rostoker Coherent Potential Approximation KKR-CPA. Experimental magnetization is also given in the last column. All values are in μ_B. Valence Electron Concentration VEC is for the number of valence electrons in a compound (see text).

Compound	VEC	Total (cal.)	Mn_{3f}	Fe_{3f}	Mn_{3g}	Fe_{3g}	Magn. (exp.)
$Mn_{1.4}Fe_{0.6}P_{0.3}Si_{0.7}$	19.0	4.25	1.76	1.48	2.82	-	4.17
$Mn_{1.3}Fe_{0.7}P_{0.35}Si_{0.65}$	19.05	3.98	1.48	1.40	2.69	-	>2.85 *
$MnFeP_{0.5}Si_{0.5}$	19.5	4.30	-	1.49	2.97	-	3.77–3.95
$Mn_{0.7}Fe_{1.3}P_{0.65}Si_{0.35}$	19.95	4.04	-	1.41	2.92	2.44	>3.25 *
$Mn_{0.6}Fe_{1.4}P_{0.6}Si_{0.4}$	20.0	3.99	-	1.43	2.91	2.42	4.05

Note: * = non-fully saturated under 7 T should be due by some AF couplings at low temperature.

Table 6. Values of magnetic moments and magnetization found for the isotype $MnFeP_{1-y}As_y$ compounds of Fe_2P type.

Compound	VEC	Total (cal.)	Mn_{3f}	Fe_{3f}	Mn_{3g}	Fe_{3g}	Magn. (exp.)
MnFeAs (HP) [10]	-	>4.23 **	-	1.10	3.13	-	4.50
$MnFeP_{0.5}As_{0.5}$	-	>3.80 **	-	1.20	2.60	-	4.13
$MnFeP_{0.7}As_{0.3}$ [14]	-	>4.27 **	-	1.25	3.02	-	4.10

Note: ** = not accounting for the slight polarization levels taking place on non-metals and at inter-sites.

However, the estimate for the Fe_{3g} magnetic moment in $Mn_{0.7}Fe_{1.3}P_{0.65}Si_{0.35}$ appears too weak for 1 µB (see Table 5). In fact, from the saturation magnetization reported Table 3, it appears that this compound could exhibit a more complex magnetic structure than assumed for KKR-CPA calculations. Alternatively, it cannot be excluded that for such complicated structures the value of the hyperfine magnetic field is not strictly proportional to the Fe magnetic moment.

3.4. Electronic Structure Analysis

3.4.1. Computational Details

Electronic structure calculations of TT′X compounds and their alloys in relation to phase stability, magnetic, and magneto-caloric properties using the Green function Korringa-Kohn-Rostoker (KKR) method, were frequently discussed in our previous papers [60–72]. The KKR method belongs to the well-established DFT techniques, as widely operated by many authors [73,74]. However, in our computations, the novel quasi-linear algorithm was implemented [75]. In turn, the KKR technique combined with the coherent potential approximation (CPA) [74] appeared to be a very efficient tool to investigate the electronic properties of chemically disordered magnetic materials. In this paper, KKR-CPA has been applied to study the electronic structure of $Mn_{1-x}Fe_xP_{1-y}Si_y$ solid solutions, aiming to enlighten their magnetic behaviors, as well as other interesting phenomena experimentally evidenced in these materials, such as the selective site substitution (Mn/Fe on 3g/3f sites and P/Si on 2c/1b sites) or the effect of a unit cell volume jump in the vicinity of Ferro-Para transition. Moreover, the spin-polarized KKR-CPA method was employed to calculate the electronic and magnetic behaviors of transition metal atoms (Mn, Fe), not only in the ferromagnetic state, but also in the so-called DLM state (disordered local moments), which can be regarded as a static model of a paramagnetic-like state. The crystal potential of the "muffin-tin" form was used, with l truncation on each atom up to l_{max} = 3. The Perdew-Wang formula describing the exchange-correlation part of the crystal potential was employed [76]. For the crystal potentials converged below 0.1 mRy, spin-polarized total, site-decomposed, and l-decomposed density of states (DOS) were computed. The Fermi level (E_F) was precisely determined from the Lloyd formula [77]. Our experimental values of the cell parameters and the atomic positions [36] were used for KKR-CPA computations (see Tables 1 and 2). More theoretical details on KKR-CPA methodology can be found elsewhere [78].

3.4.2. Site Preference

$Mn_{0.6}Fe_{1.4}P_{0.6}Si_{0.4}$ seems to be the right case, allowing the study of the selective occupancy of Fe, substituting Mn either on tetrahedral (3f) or pyramidal (3g) sites. For this purpose, three cases have been considered for the KKR-CPA total energy analysis:

(i)   0.9 Fe and 0.1 Mn on 3f, 0.5 Fe and 0.5 Mn on 3g;
(ii)   1.0 Fe on 3f, 0.4 Fe and 0.6 Mn on 3g;
(iii) fully random distribution of TM elements, i.e., 0.5 Fe and 0.5 Mn on 3f and 3g sites.

The lowest total energy was calculated for (ii) Fe/Mn distribution, while the other models of transition atoms occupancy were found to be less favorable due to the total energy (per atom) of 16 meV and 47 meV higher for (i) and (iii) models, respectively.

The KKR-CPA results remain in excellent agreement with experimental observation, showing that Fe atoms introduced in the hexagonal structure of $Mn_{2-x}Fe_xP_{1-y}Si_y$ first occupy the tetrahedral 3f site, and when the latter are entirely filled (x > 1), the rest of Fe atoms go to the pyramidal 3g site. To some extent, the selectivity of the site occupancy for iron can be explained by comparing the site-decomposed DOS sites, as shown in Figure 13 for Fe and Mn on 3f and 3g. From calculations, it appears that it is energetically more beneficial for Fe atoms to substitute Mn on 3f than on the 3g site, since DOS shapes of Fe and Mn better match on 3f over a wide range of energy (well seen for spin-up electrons).

Also, the spin-down *d*-Fe DOS peak appearing near the Fermi level is much larger for the 3g site than the corresponding one on the 3f site.
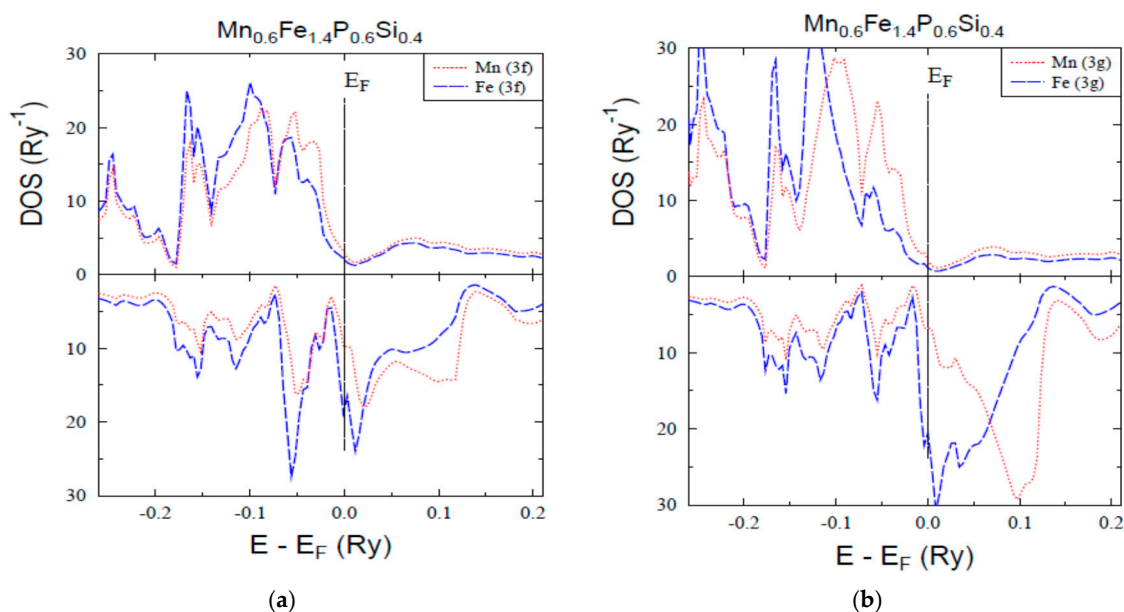
Figure 13. Density of states calculated for Mn and Fe in $Mn_{0.6}Fe_{1.4}P_{0.6}Si_{0.4}$ (**a**) for Mn and Fe on 3f sites and (**b**) for Mn and Fe on 3g sites.

The latter corresponds to a more favorable situation from an energetic point of view. The site preference of Si substituting P was analyzed in the $MnFeP_{0.5}Si_{0.5}$ compound by considering three models of atoms distribution:

(i)   0.75 P and 0.25 Si on 2c, 1.0 Si on 1b;

(ii)   0.25 P and 0.75 Si on 2c, 1.0 P on 1b;

(iii)   fully random distribution of both metalloids, i.e., 0.5 P and 0.5 Si on 2c and 1b sites.

The lowest energy was computed for configuration (ii), where Si occupies only the 2c site. The P/Si distribution within models (iii) and (i) are energetically less favorable, since the computed total energy is 16 meV and 36 meV higher, respectively. This KKR-CPA result is also well supported by the XRD refinement of the $MnFeP_{0.5}Si_{0.5}$ compound, evidencing the fact that Si atoms exclusively occupy the 2c site.

3.4.3. Magnetic Properties of $Mn_{2-x}Fe_xP_{1-y}Si_y$

Spin-polarized KKR-CPA calculations were performed for the following compounds: $Mn_{0.6}Fe_{1.4}P_{0.6}Si_{0.4}$, $Mn_{0.7}Fe_{1.3}P_{0.65}Si_{0.35}$, $MnFeP_{0.5}Si_{0.5}$, $Mn_{1.3}Fe_{0.7}P_{0.35}Si_{0.65}$, $Mn_{1.4}Fe_{0.6}P_{0.3}Si_{0.7}$, $MnFeP_{0.5}Si_{0.5}$. It is worthy to note that due to markedly different magnetic moments carried by the same

elements occupying either 3f or 3g sites, it is expected that overall magnetic behaviors should depend on the relative concentration of Fe and Mn elements. On the other hand, the influence of the relative P and Si contents on magnetic behaviors seems to be less obvious. However, we will show that both factors play an important role in the formation of $Mn_{2-x}Fe_xP_{1-y}Si_y$ magnetic characteristics, since the phosphorus differs by the number of electrons from the silicon by one, while only the transition metal atoms carry important magnetic moments. Hence, while the substitution of Mn by Fe mainly leads to the replacement of a stronger magnetic moment (~2.9 μ_B on 3g) by a slightly weaker one (~2.4 μ_B on 3g), the change in the mutual concentration of elements at the non-metal position (P/Si) leads to E_F "scanning" on the existing polarized DOS function due to the change in the number of electrons in the system.

In this sense, the valence electron count (VEC) seems to be a useful quantity that enables us to simplify the comparison between the magnetic properties of $Mn_{2-x}Fe_xP_{1-y}Si_y$ with different concentrations. Consequently, the aforementioned features result in quite complex variations of electronic and magnetic properties, depending on the alloy composition. Although the change of VEC from 19.95 ($Mn_{0.6}Fe_{1.4}P_{0.6}Si_{0.4}$) to 20 ($Mn_{1.3}Fe_{0.7}P_{0.35}Si_{0.65}$) does not significantly impact the magnetization, nevertheless the behavior of electrons near the Fermi energy is clearly different (see Figures 14 and 15).
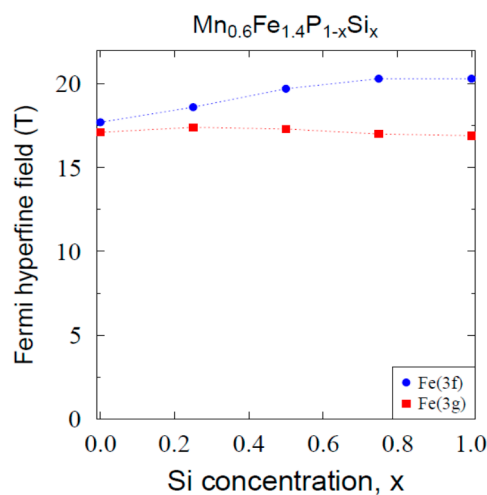
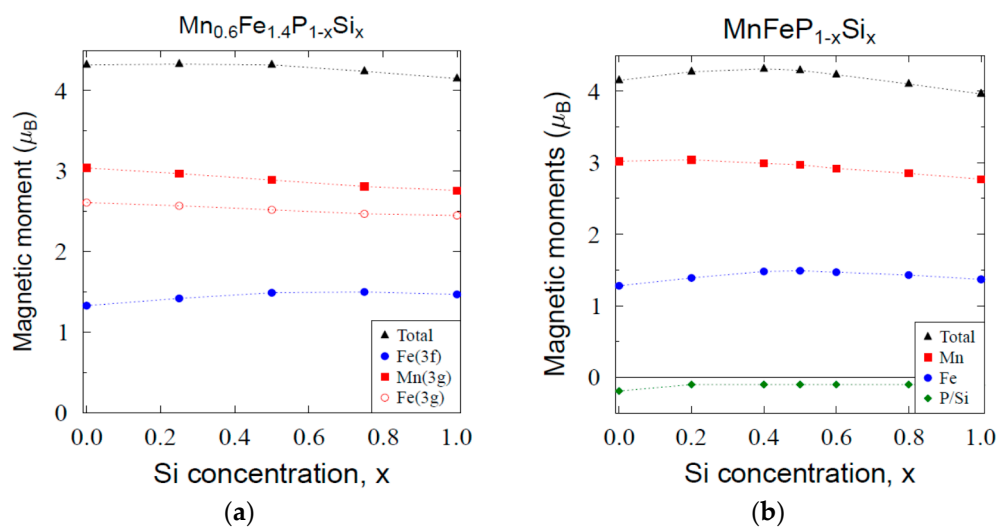**Figure 14.** Hyperfine field versus Si concentration in $Mn_{0.6}Fe_{1.4}P_{1-x}Si_x$.

Figure 15. Magnetic moments versus Si concentration in (**a**) $Mn_{0.6}Fe_{1.4}P_{1-x}Si_x$ and (**b**) $MnFeP_{1-x}Si_x$.

4. Conclusions and Perspectives

Both the parent $Mn_{2-x}Fe_xP_{1-y}As_y$ and $Mn_{2-x}Fe_xP_{1-y}Si_y$ series of compounds that exhibit peculiar and various magnetic properties and specific compositions with the hexagonal Fe_2P structure-type were demonstrated, sharing high magnetocaloric performances. The present challenges remain as: (1) contribute to fundamental knowledge for both series and (2) optimize the synthesis routes to deliver materials for magnetic refrigeration applications, namely the second series without the non-friend arsenic element. Here, it is shown that starting from defined proportions of the three base precursors that are Fe-P, Mn_5Si_3, and Mn_3Si, combined with tiny amounts of elements such as Fe, Co, and Ge to refine the balance, the synthesis of the desired magnetocaloric performing formula can be easily achieved using a conventional high frequency melting process. Moreover, such a process can be up-scaled up to 10 kg batches.

The present paper focuses on five selected formula, namely $Mn_{1.40}Fe_{0.60}P_{0.30}Si_{0.70}$, $Mn_{1.30}Fe_{0.70}P_{0.35}Si_{0.65}$, $MnFeP_{0.50}Si_{0.50}$, $Mn_{0.70}Fe_{1.30}P_{0.65}Si_{0.35}$, and $Mn_{0.60}\ Fe_{1.40}P_{0.60}Si_{0.40}$ from the Mn-rich side to the Fe-rich side. At the same time, the non-metal composition was chosen according to the metal one. Crystalline structure investigations were systematically conducted on the series of Mn-Fe phosphide-silicides, allowing retrieval of the strong magnetoelastic phenomena accompanying the Ferro-Antiferromagnetic and Ferro-Paramagnetic transformations, as pointed out earlier in the hexagonal Mn-Fe phosphide-arsenide series [4,14–16], and already pointed out elsewhere [25]. It was confirmed that again in the new series (P-Si), Mn(3g) and Fe(3f) prefer to occupy pyramidal (CN5) and tetrahedral (CN4) sites, respectively [25,36]. At the same time, the Si stoichiometry cannot overpass the ratio $Si/P = \frac{1}{2}$, since the non-metal have to be repatriated into 2c and 1b positions of the hexagonal P-62m space group. This selective occupancy of Si results from steric consideration, since as mentioned above, PYR volume = 2 TET volume. In this context, it is worthy to remember that for the isotype $Mn_{2-x}Fe_xP_{1-y}As_y$ system [4,14], the hexagonal domain composition is limited to y = 0.66.

Systematic studies devoted to the TT'X series (T and T' = transition metals, X = P, As, Si, Ge), have enabled characterization of most of the hexagonal-type compounds exhibiting ferromagnetic characteristics, where magnetoelastic phenomena [4,14–16,25–29,34], up to a change in the crystal structure [79,80], accompany the change or the loss of magnetic exchange couplings. Three causes can be considered: (1) the preferential presence of Fe in the "smaller" TET site with rather short Fe-X distances; (2) the sensibility of the Fe moment (discussed in [42,44]) as a magnetic element at the limit of weak to strong ferromagnetic behavior; and (3) the layered metal/non-metal disposition in the successive [001]-planes, with Mn-P alternating to Fe-Si containing layers. The combination of these three factors leads to certain instability in the local magnetic polarization of Fe, and then in the Fe–Fe (and Fe–Mn) long- and short-range exchange couplings. Therefore, here it is proposed to consider a new index of local striction effect, expressed as $\delta = dp/da - 1$, to be directly related to the strength of the magnetoelastic effect accompanying the change or the loss of Fe–Fe ferromagnetic correlations. Specifically, this concerns the tetrahedral site only, Fe dominantly occupying the 3f position, where *dp* expresses the variation in the 1b–1b distance (here only occupied by P atoms), and *da* expresses the variation in the 2c–2c distance (occupied by Si and P, in reference to the y value). In fact, the δ index refers to the relative elongation/contraction of the CN4 tetrahedral environment of the Fe planar/axial, according to the main axis of the structure. As a consequence, recalling Figures 3–5, the thermal variation $\delta(T)$ leads to anticipation of the behavior of (T) and c (T) cell parameters at the first order magnetic transition. Since in these metal-type materials, the ionicity degree of the elements is not particularly marked, there are no specific reference T-X (T'-X) distances as there are for oxides and halides. Consequently, the full lattice relaxes smoothly at the transition when no marked magneto-volume phenomenon is observed. No abrupt changes, such as the measured *d*(T) along the magnetic transition in the parent orthorhombic series of TT'X compounds, were noted.

The induction melting synthesized compounds exhibit a well-defined magnetocaloric performance, as determined from ΔS_m and ΔT_{ad} measurements, which are the magnetic entropy and adiabatic temperature variations over the first order magnetic transition region. Concerning this

point, we are aware that the presence of large hysteretic effects, combined with the inappropriate use of the Maxwell relation, would overestimate the entropy change exhibited by some samples [81]. This question will be addressed in a forthcoming communication. On the other hand, if the HF melting process appears a rather easy one, the homogenization procedure via a carefully executed annealing step remains mandatory to expect optimized performances. In support of the more fundamental analyses undertaken here to qualify the crystal and magnetic characteristics of the series, ^{57}Fe Mössbauer spectroscopy measurements and electronic structure calculations were developed. Three compositions were analyzed by using the ^{57}Fe Mössbauer spectroscopy: a Mn-rich, the Mn/Fe equi-atomic, and a Fe-rich formula. Interestingly, the local coordination in non-metal elements was found not essentially critical in terms of local polarization. The magnetic interactions with the number of next Fe neighbors played the most important role. In fact, the spectra were fairly decomposed in their different components, allowing allocation to the Fe_{3f} and Fe_{3g} well defined values, in agreement with obtained calculations from the electronic structure determination. This approach was used to compare the possible scheme of metal and non-metal crystallographic ordering. Unambiguously, it was confirmed that the Mn/Fe preferential occupations are for the 3g and 3f sites, respectively, while the P and Si preferential occupations are for the 1b and 2c sites, respectively.

The 3g moments on the PYR sites (either Mn only or Mn/Fe occupied) appear weakly decreased by the Si content, de facto up to y = 0.66. A similar situation occurs for the Fe_{3f} moment of the TET sites, with an increasing tendency. However, if both calculated variations remained rather limited, the values calculated for the Fe magnetic moments that were related to the 3f and 3g sites agree well with those found by Mössbauer spectroscopy, and the as-calculated total magnetization values were in fair agreement with the experimental values deduced from experimental magnetization measurements. Meanwhile, in spite of the large similarities in terms of numerical values for the local and global magnetic characteristics, the density of states calculated for Mn and Fe in $MnFeP_{0.5}Si_{0.5}$ are significantly different and determine the effective attribution of the metal elements in one (3f) or the other (3g) site. All the fundamental characteristics, either experimentally or theoretically determined in the present analysis for various members of the $Mn_{2-x}Fe_xP_{1-y}Si_y$ series, appear coherent, along with the multiple data from the reported literature.

Author Contributions: D.F. works as a solid state chemist and physicist (e.g., on magnetic and magnetocaloric materials), and participated in the synthesis, crystal structure, and magnetic analyses. He also supervised the work of S.H.-K. as PhD, and has written the original draft manuscript in direct collaboration with all contributors. S.H-K. participated in the synthesis, XRD collection, and bulk magnetic and Cp measurements up to their global analysis. P.d.R. works as a solid state chemist and physicist (e.g., on magnetic materials) and participated in the RT XRD measurements and SEM microscopy analysis. She was actively involved in the management of the S.H.-K. works. M.B. is a specialist of magnetocaloric materials and the analysis of their experimental properties and namely of the formal modeling of transition metal pnictides comprising the series MnFe(P,X). He participated in the evolution of the drafted manuscript. R.Z. is a solid state physicist working on thermodynamics of magnetic metal systems versus temperature and pressure. He validated the crystal structure and magnetic property investigations versus temperature. W.C. works as a PhD of R.Z. and recorded the XRD data and then analyzed the cell parameter behaviors versus temperature by using profile refinements methods. P.F. is a solid state physicist using ^{57}Fe Mössbauer spectroscopy and other methods for interpreting the bulk and dynamics of systems at micro- to atomic-scales (e.g., he is a specialist of thermal behavior of hyperfine parameters). J.S. is a solid state physicist, specialized in ^{57}Fe Mössbauer spectroscopy, thus building and managing the used experimental set-up. He has fitted and interpreted the resulting data. S.K. (†) is a solid state and theoretical physicist, who has for a time developed and continuously improved very powerful codes for KKR-CPA calculations. He was actively associated in the present analysis, leading to clear-cut results. J.T. is a solid state physicist strongly involved in the present and related investigations on theoretical magnetic characterization on intermetallic compounds, allowing establish a relationship between bulk and atomic-scale peculiarities, with nuclear and hyperfine characteristics.
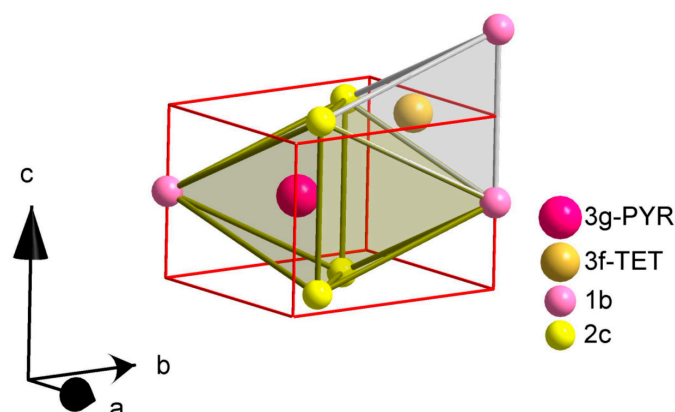
Appendix A

Figure A1. The crystal structure of the $Mn_{2-x}Fe_xP_{1-y}Si_y$ compounds (Fe_2P type, SG P-62m), showing the environments of the two metal sites (3f for TET, 3g for PYR) and the two non-metal sites at 1b and 2c positions. In fact, the index $\delta = d_{(2c\text{-}2c)}/c - 1$ is determined from the ratio of planar (p) and axial (a) edges of the tetrahedral site (TET).

Table A1. A comparison of interatomic distances for two selected parent systems.

	Interatomic Distances at 290 K [Å]	
	$MnFeP_{0.5}Si_{0.5}$	$Mn_{0.6}Fe_{1.4}P_{0.6}Si_{0.4}$
Mn-Mn	3.267 x4	3.233 x4
Mn-Fe	2.716 x2 2.740 x4	2.619 x2 2.737 x2
Mn-P,Si **Mn-P**	2.509 x4 2.499 x1	2.503 x4 2.461 x1
Fe-P,Si **Fe-P**	2.371 x2 2.267 x2	2.268 x2 2.339 x2
Fe-Fe	2.673 x2	2.642 x2

In fact, a direct and significant comparison is not obvious, because of the two species changing composition, and, moreover, due to the magnet–elastic effect, the changes must be expressed in an absolute temperature scale with reference to the ordering temperature that could higher or lower than RT. With substitution of Fe to Mn, the P-P and P,Si-P distances decrease by less than 1%. However the most marked changes are concerned the tetrahedral site containing iron, as it was found first for the $Mn_{1-x}Fe_xP_{1-y}As_y$ systems [14–16].

Table A2. A comparison of interatomic distances for $MnFeP_{0.5}Si_{0.at}$ temperatures apart T_C.

	300 K (F)	465 K (P)
Mn-Mn	3.262 x4	3.203 x4
Mn-Fe	2.691 x2 2.758 x4	2.689 x2 2.763 x4
Mn-P	2.505 x2 2.505 x2 2.528 x1	2.533 x2 2.534 x2 2.455 x1
Fe-P	2.371 x2 2.267 x2	2.291 x2 2.335 x2
Fe-Fe	2.689 x2	2.712 x2

Once again, the interatomic distances related to the tetrahedra are revealed as sensitive to the magnetoelastic phenomenon. However, in all cases, the TET site is deformed but its volume varies by less than 2×10^{-2} Å^3, similarly to the relative cell volume variation $\Delta V/V$ at transition, as shown in the Figure 5. Besides the axial Mn-P distance decrease, the paramagnetic Mn shifts by ~0.075 Å towards the apex of the PYR site. Correspondingly, the nearest Mn–Mn distances decrease by symmetry for ~0.06 Å. This is fully coherent with the TET deformation expressed by the index $\delta = d_{(2c\text{-}2c)}/c - 1$ as a driving force of the magnetoelastic distortion, with the a-cell parameter dropping down at T_C conversely to the drop up of the c-cell parameter.
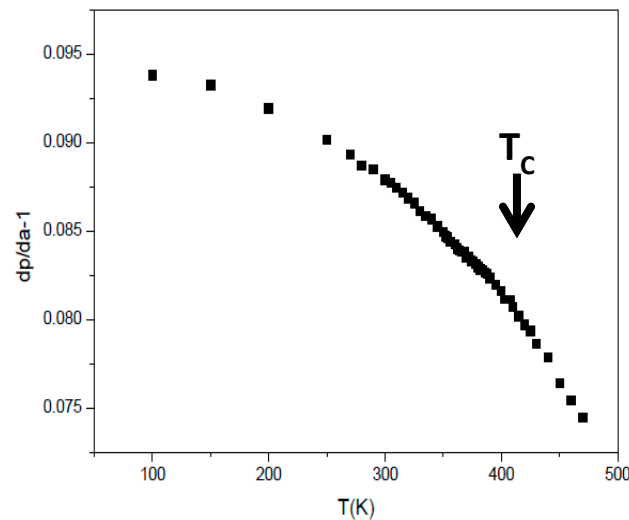
Figure A2. Example of a smooth transition in the parent compound MnFeP$_{0.5}$Si$_{0.5}$, directly received from atomization and ferromagnetically ordering close to the 390–400 K Plot of the $\delta = d_{(2c\text{-}2c)}/c - 1$ index versus temperature shows no noticeable magnetoelastic effect. leading to almost no variation of magnetic entropy at transition as reported in Figure 11. In fact, this atomized material exhibits ~12% of Mn$_3$Fe$_2$Si$_3$ as impurity and some atomic disorders in the Fe$_2$P-type structure, preventing an established collective magnetoelastic phenomenon.

References

1. Fruchart, R. Effets d'électronégativité et interactions métalliques dans les phosphures et arséniures ternaires des éléments de transition 3d, 4d, 5d de type métallique. *Annales de Chimie* **1982**, *7*, 563–604. (In French)
2. Beckman, O.; Lundgren, L. Compounds of transition elements with nonmetals. *Hand. Magn. Mater.* **1991**, *6*, 181–287.
3. Fruchart, D.; Wolfers, P. Chalcogenides and Pnictides. In *Handbook of Magnetic and Advanced Magnetic Materials (HMM)*; Krönmuller, H., Parkin, S., Eds.; J. Wiley and Sons: Hoboken, NJ, USA, 2007; pp. 2378–2400.
4. Krumbuguel-Nylund, A. Etude Structurale et Magnétique des Arséniophosphures MM4(P$_{1-y}$As$_y$) et des Solutions Solides Entre Arséniures M$_2$As des Métaux de Transitions de la Première Série (M,M′ = Cr, Mn, Fe, Co, Ni). Ph.D. Thesis, Université Paris-Orsay, Orsay, France, 1974. (In French)
5. Yoshii, S.; Katsuraki, H. Neutron Diffraction Study of FeMnAs. *J. Phys. Soc. Japan* **1967**, *22*, 674. [CrossRef]
6. Roger, A. Etude Cristallographique et Magnétique des Phosphures MP et M$_2$P de la Série du fer et de Leurs Solutions Solides. Ph.D. Thesis, Université de Paris, Paris, France, 1970. (In French)
7. Chenevier, B. Etude des Transitions de Phases Cristallines et Magnétiques Dans les Systèmes Fe$_2$P-Mn$_2$P, MnRuAs, MnRhAs et FeRhP. Ph.D. Thesis, Université J. Fourier, Grenoble, France, 1990. (In French)
8. Suzuki, T.; Yamaguchi, Y.; Yamamoto, H.; Watanabe, H. Magnetic Structure of FeMnP. *J. Phys. Soc. Jpn.* **1973**, *34*, 911–916. [CrossRef]
9. Chenevier, B.; Soubeyroux, J.L.; Bacmann, M.; Fruchart, D.; Fruchart, R. The high temperature orthorhombic-hexagonal phase transformation of FeMnP. *Sol. State Commun.* **1987**, *64*, 57–61. [CrossRef]

10. Tobola, J.; Bacmann, M.; Fruchart, D.; Wolfers, P.; Kaprzyk, S.; Koumina, A.A. Structure and magnetism in the polymorphous MnFeAs. *J. Alloys Compd.* **2001**, *317*, 274–279. [CrossRef]

11. Senateur, J.P.; Rouault, A.; Fruchart, R.; Capponi, J.J.; Perroux, M. Etude par spectrométrie Mössbauer des transformations cristallographiques sous hautes pressions de MnFeAs et Fe_2P. *Mat. Res. Bull.* **1976**, *11*, 631–635. (In French) [CrossRef]

12. Roy, P. Treatise on Magnetocaloric MnFe(Si,P) Compounds: A First-Principles Study. Ph.D. Thesis, Radboud University, Nijmegen, The Netherlands, 2016.

13. Sénateur, J.P.; Fruchart, D.; Boursier, D.; Rouault, A.; Montreuil, J.R.; Deyris, B. Analyse des facteurs d'ordre des matériaux de transition dans les phosphures et arséniures MM'P et MM'As. *J. Phys. Coll.* **1977**, *38*, 61–70. (In French)

14. Bacmann, M.; Soubeyroux, J.L.; Barrett, R.; Fruchart, D.; Zach, R.; Niziol, S.; Fruchart, R. Magnetoelastic transition and antiferro-ferromagnetic ordering in the system $MnFeP_{1-y}As_y$. *J. Magn. Magn. Mater.* **1994**, *134*, 59–67. [CrossRef]

15. Malaman, B.; Le Caër, G.; Delcroix, P.; Fruchart, D.; Bacmann, M.; Fruchart, R. Magneto-elastic transition and magnetic couplings: A Mössbauer spectroscopy study of the system. *J. Phys. Cond. Matter* **1996**, *8*, 8653. [CrossRef]

16. Zach, R.; Niziol, S.; Karpzyk, S.; Tobola, J.; Bacmann, M.; Fruchart, D.; Fruchart, R.; Wolfers, P. Magnetoelastic properties of $MnFeP_{1-y}As_y$ and band structure results from KKR-CPA. *Acta Phys. Pol.* **1997**, *A91*, 471–477. [CrossRef]

17. Hermann, R.P.; Tegus, O.; Brück, E.; Buschow, K.H.J.; De Boer, F.R.; Long, G.J.; Grandjean, F. Mössbauer spectral study of the magnetocaloric $FeMnP_{1-x}As_x$ compounds. *Phys. Rev. B* **2004**, *70*, 214425. [CrossRef]

18. Sénateur, J.P.; Madar, R.; Fruchart, R.; Fruchart, D.; Auric, P. Interpretation of the ambiguous Mössbauer spectra of Fe_2P: Study of a $^{57}Co/Fe_2P$ source. In Proceedings of the VI International Conference on Solid Compounds of Transition Elements, Stuttgart, Germany, 12–16 June 1979; pp. 88–191.

19. Ericsson, T.; Häggström, L.; Wäppling, R.; Methasiri, T. Mössbauer spectroscopic study of Fe_2P with Cu impurities. *Phys. Scripta* **1980**, *21*, 212. [CrossRef]

20. Wiendlocha, B.; Tobola, J.; Kaprzyk, S.; Zach, R.; Hlil, E.K.; Fruchart, D. Magnetocaloric properties of $Fe_{2-x}T_xP$ (T = Ru and Rh) from electronic structure calculations and magnetization measurements. *J. Phys. D Appl. Phys.* **2008**, *41*, 205007. [CrossRef]

21. Tobola, J. Study of Intermetallic Compounds Containing Iron by Band Theory Methods. Ph.D. Thesis, AGH Krakow, Kraków, Poland, 1994.

22. Moriya, T. Spin fluctuations in ferromagnetic metals—Temperature variation of local moment and short-range order. *J. Phys. Soc. Japan* **1982**, *51*, 420–434. [CrossRef]

23. Miao, X.F.; Caron, L.; Gubbens, P.C.M.; Yaouanc, A.; de Réotier, P.D.; Luetkens, H.; Brück, E. Spin correlations in (Mn,Fe)$_2$(P,Si) magnetocaloric compounds above Curie temperature. *J. Sci. Adv. Mater. Devices* **2016**, *1*, 147–151. [CrossRef]

24. Haj-Khlifa, S.; de Rango, P.; Fruchart, D.; Zach, R. Crystal and magnetic effects of selected substitutions of Ni for Fe and for Co in the orthorhombic $MnFe_{0.35}Co_{0.65}P$ compound. *J. Alloys Compd.* **2015**, *652*, 322–330. [CrossRef]

25. Tegus, O.; Brück, E.; Buschow, K.H.J.; de Boer, F.R. Transition-metal-based magnetic refrigerants for room-temperature applications. *Nature* **2002**, *415*, 150. [CrossRef]

26. Tegus, O.; Brück, E.; Zhang, L.; Buschow, K.H.J.; de Boer, F.R. Magnetic-phase transitions and magnetocaloric effects. *Phys. B Cond. Matter* **2002**, *319*, 174–192. [CrossRef]

27. Koyama, K.; Kanomata, T.; Watanabe, K. High field X-ray diffraction studies on $MnFeP_{0.5}As_{0.5}$. *Japan. J. Appl. Phys.* **2005**, *44*, L549. [CrossRef]

28. Yue, M.; Li, Z.Q.; Wang, X.L.; Liu, D.M.; Zhang, J.X.; Liu, X.B. Crystal structure and magnetic transition of MnFePGe compound prepared by spark plasma sintering. *J. Appl. Phys.* **2009**, *105*, 7A915. [CrossRef]

29. Yibole, H.; Guillou, F.; Huang, Y.K.; Blake, G.R.; Lefering, A.J.E.; van Dijk, N.H.; Brück, E. First-order ferromagnetic transition in single-crystalline (Mn,Fe)$_2$(P,Si). *Appl. Phys. Lett.* **2015**, *107*, 162403. [CrossRef]

30. Höglin, V.; Hudl, M.; Caron, L.; Beran, P.; Sørby, M.H.; Nordblad, P.; Sahlberg, M. Detailed study of the magnetic ordering in $FeMnP_{0.75}Si_{0.25}$. *J. Solid State Chem.* **2015**, *221*, 240–246. [CrossRef]

31. Guillou, F.; Ollefs, K.; Wilhelm, F.; Rogalev, A.; Yaresko, A.N.; Yibole, H.; Brück, E. Electronic and magnetic properties of phosphorus across the first-order ferromagnetic transition of $(Mn,Fe)_2(P, Si, B)$ giant magnetocaloric materials. *Phys. Rev. B* **2015**, *92*, 224427. [CrossRef]

32. Delczeg-Czirjak, E.K.; Pereiro, M.; Bergqvist, L.; Kvashnin, Y.O.; Di Marco, I.; Li, G.; Eriksson, O. Origin of the magnetostructural coupling in $FeMnP_{0.75}Si_{0.25}$. *Phys. Rev. B* **2014**, *90*, 214436. [CrossRef]

33. Okamoto, H. The Iron Phosphorus (Fe-P) System. *ASM Int. Bull. Alloy Diagr.* **1990**, *11*, 4. [CrossRef]

34. Sandeman, K.G. Magnetocaloric materials: The search for new systems. *Scripta Mater.* **2012**, *67*, 566–571. [CrossRef]

35. Mayer, C.; Pierronnet, M. (Erasteel SAS, 33 avenue du Maine, 75755 Paris Cedex 15, France). Private communication, 2014.

36. Khadechi-Haj Khlifa, S. Propriétés Structurales, Magnétiques et Magnétocaloriques de Pnictures Isotypes de Mn (Fe, Co) P. Ph.D. Thesis, Université Grenoble Alpes, Grenoble, France, 2016. (In French)

37. Luo, J. (Xian PureMetals Advanced Materials Ltd., 40-3-502 Erfuzhuang Zone Zhengfa Xiang, Weiyang Road, Xian City, Shaanxi Province 720016, China). Personal communication, 2018.

38. Meisner, G.P. The Superconductivity, Structure, and Magnetism of Some Ternary Transition Metal Phosphides and Arsenides. Ph.D. Thesis, University of California, San Diego, CA, USA, 1983.

39. Boeije, M.F.J.; Maschek, M.; Miao, X.F.; Thang, N.V.; van Dijk, N.H.; Brück, E. Mixed magnetism in magnetocaloric materials with first-order and second-order magnetoelastic transitions. *J. Phys. D Appl. Phys.* **2017**, *50*, 174002. [CrossRef]

40. Wurentuya, B.; Yibole, H.; Guillou, F.; Ou, Z.; Zhang, Z.; Tegus, O. First-order magnetic transition, magnetocaloric effect and moment formation in MnFe(P,Ge) magnetocaloric materials revisited by x-ray magnetic circular dichroism. *Phys. B. Cond. Matter* **2018**, *544*, 66–72. [CrossRef]

41. Cam Thanh, T.; Brück, E.; Trung, N.T.; Klaasse, J.C.P.; Buschow, K.H.J.; Ou, Z.Q.; Tegus, O.; Caron, L. Structure, magnetism, and magnetocaloric properties of $MnFeP_{1-x}Si_x$ compounds. *J. Appl. Phys.* **2008**, *103*, 7B318. [CrossRef]

42. Hudl, M.; Häggström, L.; Delczeg-Czirjak, E.K.; Höglin, V.; Sahlberg, M.; Vitos, L.; Eriksson, O.; Nordblad, P.; Andersson, Y. Strongly enhanced magnetic moments in ferromagnetic $FeMnP_{0.5}Si_{0.5}$. *Appl. Phys. Lett.* **2011**, *99*, 152502. [CrossRef]

43. Dung, N.H.; Zhang, L.; Ou, Z.Q.; Brück, E. Magneto-elastic coupling and magnetocaloric effect in hexagonal Mn-Fe-P-Si compounds. *Scripta Mater.* **2012**, *67*, 975–978. [CrossRef]

44. Dung, N.H.; Zhang, L.; Ou, Z.Q.; Zhao, L.; van Eijck, L.; Mulders, A.M.; Avdeev, M.; Suard, E.; van Dijk, N.H.; Bruck, E. High/low-moment phase transition in hexagonal Mn-Fe-P-Si compounds. *Phys. Rev. B* **2012**, *86*, 045134. [CrossRef]

45. Höglin, V.; Cedervall, J.; Andersson, M.S.; Sarkar, T.; Nordblad, P.; Sahlberg, M. Irreversible structure change of the as prepared $FeMnP_{1-x}Si_x$ structure on the initial cooling through the Curie Temperature. *J. Magn. Magn. Mater.* **2015**, *374*, 455–458.

46. Christiaanse, T.V.; Campbell, O.; Trevizoli, P.V.; Misra, S.; van Asten, D.; Zhang, L.; Govindappa, P.; Niknia, I.; Teyber, R.; Rowe, A. A concise approach for building the s-T diagram for Mn-Fe-P-Si hysteretic magnetocaloric material. *J. Phys. D Appl. Phys.* **2017**, *50*, 365001. [CrossRef]

47. Fries, M.; Pfeuffer, L.; Bruder, E.; Gottschall, T.; Ener, S.; Diop Lé, V.B.; Gröb, T.; Skokov, K.P.; Gutfleisch, O. Microstructural and magnetic properties of Mn-Fe-P-Si (Fe_2P-type) magnetocaloric compounds. *Acta Mater.* **2017**, *132*, 222–229. [CrossRef]

48. He, A.; Svitlyk, V.; Mozharivskyj, Y. Synthetic Approach for $(Mn,Fe)_2(Si,P)$ Magnetocaloric Materials: Purity, Structural, Magnetic, and Magnetocaloric Properties. *Inorg. Chem.* **2017**, *56*, 2827–2833. [CrossRef]

49. Miao, X.F.; Hu, S.Y.; Xu, F.; Ekkes Bruck, E. Overview of magnetoelastic coupling in $(Mn, Fe)_2(P,Si)$-type magnetocaloric materials. *Rare Metals* **2018**, *37*, 723–733. [CrossRef]

50. Balli, M.; Fruchart, D.; Zach, R. Negative and conventional magnetocaloric effects of a MnRhAs single crystal. *J. Appl. Phys.* **2014**, *115*, 203909. [CrossRef]

51. Balli, M.; Jandl, S.; Fournier, P.; Kedous-Lebouc, A. Advanced materials for magnetic cooling: Fundamentals and practical aspects. *Appl. Phys. Rev.* **2017**, *4*, 021305. [CrossRef]

52. Pecharsky, V.K.; Gschneidner, K.A., Jr. Magnetocaloric effect from indirect measurements: Magnetization and heat capacity. *J. Appl. Phys.* **1999**, *86*, 565–575. [CrossRef]

53. Rosca, M. Matériaux de Type LaFe$_{13-x}$Si$_x$ à Fort Pouvoir Magnétocalorique-Synthèse et Optimisation de Composés Massifs et Hypertrempés—Caractérisations Fondamentales. Ph.D. Thesis, Université de Grenoble, Grenoble, France, 2010. (In French)

54. Zach, R.; Tobola, J.; Sredniawa, B.; Kaprzyk, S.; Guillot, M.; Fruchart, D.; Wolfers, P. Magnetic interactions in the MnFe$_{1-x}$Co$_x$P series of solid solutions. *J. Phys. Cond. Matter* **2007**, *19*, 376201. [CrossRef]

55. Średniawa, B.; Zach, R.; Fornal, P.; Duraj, R.; Bombik, A.; Tobola, J.; Fruchart, D. Crystal structure, magnetic and electronic properties of Co$_x$Fe$_{1-x}$MnP system. *J. Alloys Compd.* **2001**, *317*, 266–273. [CrossRef]

56. Zach, R.; Tobola, J.; Chajec, W.; Fruchart, D.; Ono, F. Magnetic properties of MM'X (M = Mn, M' = 3d or 4d metal, X = P, As, Si, Ge) compounds with hexagonal or orthorhombic crystal structure. *Sol. State Phenom.* **2013**, *194*, 98–103. [CrossRef]

57. Zach, R. Magnetic Properties and Magnetoelastic Phase Transitions of MnFeP$_{1-x}$As$_x$ (0.15 < x < 0.66) and MnRhP$_{1-x}$As$_x$ Isostructural Series of Solid Solutions. Habilitation Thesis, Zeszyty Naukowe Politechnika Krakowska, Kraków, Poland, 1997.

58. Mitsiuk, V.I.; Tkachenka, T.M.; Budzynski, M.; Surowiec, Z.; Valkov, V.I. Mössbauer investigations of Mn$_{2-x}$Fe$_x$P$_{0.5}$As$_{0.5}$. *Nukleonika* **2013**, *58*, 169–172.

59. Dubiel, S.M. Relationship between the magnetic hyperfine field and the magnetic moment. *J. Alloys Compd.* **2009**, *488*, 18–22. [CrossRef]

60. Tobola, J.; Bacmann, M.; Fruchart, D.; Kaprzyk, S.; Koumina, A.; Niziol, S.; Zach, R. Magnetism of Fe$_2$P investigated by neutron experiments and band structure calculations. *J. Mag. Mag. Mat.* **1996**, *157*, 708–710. [CrossRef]

61. Kaprzyk, S.; Niziol, S.; Tobola, J.; Zach, R.; Bacmann, M.; Fruchart, D.; Wolfers, P. Magnetic and transport properties of (Fe$_{1-x}$Ni$_x$)$_2$P in view of KKR-CPA results. *Acta Phys. Pol. A* **1997**, *91*, 475. [CrossRef]

62. Tobola, J.; Kapryzk, S.; Fruchart, D.; Bacmann, M.; Wolfers, P.; Fruchart, R. Electronic and magnetic structure of ternary transition metal arsenides related to the Fe$_2$X type (X = P, As). *J. Alloys Compd.* **1997**, *262*, 65–70. [CrossRef]

63. Zach, R.; Bacmann, M.; Fruchart, D.; Wolfers, P.; Fruchart, R.; Guillot, M.; Tobola, J. Magneto-elastic properties of MnFeP$_{1-x}$As$_x$ (0.15 ≤ x ≤ 0.66) and MnRhP$_{1-x}$As$_x$ isostructural series of compounds. *J. Alloys Compd.* **1997**, *262*, 508–511. [CrossRef]

64. Zach, R.; Guillot, M.; Tobola, J. Semiquantitative analysis of magnetic phase transitions in the MnFeP$_{1-x}$As$_x$ series of compounds. *J. Appl. Phys.* **1998**, *83*, 7237–7239. [CrossRef]

65. Sredniawa, B.; Zach, R.; Fornal, P.; Duraj, R.; Bombik, A.; Tobola, J.; Kaprzyk, S.; Nizioł, S.; Fruchart, D.; Bacmann, M.; et al. Crystal structure, magnetic properties of Co(Mn-Fe)P system. *J. Alloys Compd.* **2001**, *317–318*, 218–223.

66. Sredniawa, B.; Zach, R.; Chajec, W.; Duraj, R.; Tobola, J.; Niziol, S.; Fruchart, D.; Bacmann, M. Magnetism and electronic structure of the (Co$_{1-x}$Mn$_x$)$_2$P system. *J. Magn. Mag. Mat.* **2002**, *242*, 931–934. [CrossRef]

67. Zach, R.; Tobola, J.; Sredniawa, B.; Kaprzyk, S.; Casado, C.; Bacmann, M.; Fruchart, D. Magneto-elastic properties and electronic structure analysis of the (Fe$_{1-x}$Ni$_x$)$_2$P system. *J. Alloys Compd.* **2004**, *383*, 322–327. [CrossRef]

68. Fruchart, D.; Allab, F.; Balli, M.; Gignoux, D.; Hlil, E.K.; Koumina, A.; Zach, R. On the magnetocaloric effect in d-metal pnictides. *Phys. A Statist. Mech. Appl.* **2005**, *358*, 123–135. [CrossRef]

69. Balli, M.; Fruchart, D.; Gignoux, D.; Tobola, J.; Hlil, E.K.; Wolfers, P.; Zach, R. Magnetocaloric effect in ternary metal phosphides (Fe$_{1-x}$Ni$_x$)$_2$P. *J. Magn. Magn. Mat.* **2007**, *316*, 358–360. [CrossRef]

70. Zach, R.; Fukami, Y.; Tobola, J.; Ono, F.; Fruchart, D. Pressure induced state in the orthorhombic (Mn$_{1-x}$Co$_x$)$_2$P system. *J. Phys. Cond. Matter* **2008**, *20*, 195207. [CrossRef]

71. Zach, R.; Chajec, W.; Tobola, J.; Fruchart, D.; Hlil, E.K.; Balli, M.; Wolfers, P. Magnetic properties and magnetocaloric effect in selected MM'X-type (M, M' = 3d or 4d metal, X = As, P, Ge) and Mn$_{1-x}$T$_x$As-type (T = 3d metal) intermetallics. *Sol. State Phenom.* **2011**, *170*, 180–184. [CrossRef]

72. Szymański, D.; Zach, R.; Chajec, W.; Duraj, R.; Tobola, J.; Guillot, M.; Fruchart, D. Magnetization, high pressure, and magnetocaloric studies of MnRu$_x$Rh$_{1-x}$As (x = 0.05, 0.1): Experimental and theoretical approaches. *J. Alloys Compd.* **2018**, *776*, 59–70.

73. Butler, W.H.; Dederichs, P.H.; Gonis, A.; Weaver, R.L. *Application of Multiple Scattering Theory to Materials Science: Volume 253 (MRS Proceedings)*; Materials Research Society: Pittsburgh, PA, USA, 1992.

74. Der Kellen, S.B.; Oh, Y.; Badralexe, E.; Freeman, A.J. Self-consistent full-potential total-energy Korringa-Kohn-Rostoker band-structure method: Application to silicon. *Phys. Rev. B* **1995**, *51*, 9560. [CrossRef]

75. Stopa, T.; Kaprzyk, S.; Toboła, J. Linear aspects of the Korringa–Kohn–Rostoker formalism. *J. Phys. Cond. Matter* **2004**, *16*, 4921. [CrossRef]

76. Perdew, J.P.; Wang, Y. Accurate and simple analytic representation of the electron-gas correlation energy. *Phys. Rev. B* **1992**, *45*, 13244. [CrossRef]

77. Kaprzyk, S.; Bansil, A. Green's function and a generalized Lloyd formula for the density of states in disordered muffin-tin alloys. *Phys. Rev. B* **1990**, *42*, 7358. [CrossRef]

78. Bansil, A.; Kaprzyk, S.; Mijnarends, P.E.; Tobola, J. Electronic structure and magnetism of $Fe_{3-x}V_xX$ (X = Si, Ga, and Al) alloys by the KKR-CPA method. *Phys. Rev. B* **1999**, *60*, 13396. [CrossRef]

79. Niziol, S.; Bombik, A.; Bazela, W.; Szytula, A.; Fruchart, D. Crystal and magnetic structure of $Co_xNi_{1-x}MnGe$ system. *J. Magn. Magn. Mater.* **1982**, *27*, 281–292. [CrossRef]

80. Niziol, S.; Binczycka, H.; Szytula, A.; Todorovic, J.; Fruchart, R.; Senateur, J.P.; Fruchart, D. Structure magnétique des MnCoSi. *Phys. Stat. Solidi (a)* **1978**, *45*, 591–597. [CrossRef]

81. Balli, M.; Fruchart, D.; Gignoux, D.; Zach, R. The "colossal" magnetocaloric effect in $Mn_{1-x}Fe_xAs$: What are we really measuring? *Appl. Phys. Lett.* **2009**, *95*, 072509. [CrossRef]